E-20-F21
3, 4

HRC FINAL REPORT

CLIMATE AND HYDROLOGIC FORECASTS AND OPERATIONAL WATER RESOURCES MANAGEMENT–CASE STUDIES: LAKE LANIER & LAKE NORRIS

(GIT SUBCONTRACT AWARD NO. E-20-F21-G1 TO NOAA NA96GP0408)

Theresa M. Carpenter and Konstantine P. Georgakakos
Hydrologic Research Center
12780 High Bluff Drive, Suite 250, San Diego, CA 92130
E-mail: KGeorgakakos@hrc-lab.org

31 August 2002

1. Introduction

In recent years, there has been increased focus on utilizing climate information and climate forecasts in water resources management. Can such information provide beneficial information to be used in the operation or management of various water resource projects? This report focuses on two studies that aim to quantitatively assess benefits that use of climate forecast has for the improved management of reservoir hydrosystems. Both studies were supported by the Office of Global Programs of the National Oceanic and Atmospheric Administration (NOAA/OGP) through NOAA Grant No. NA96GP0408 (HRC Subcontract Award: E-20-F21-G1). These were retrospective studies using historical climate forecasts and observed data, and involved collaboration between a forecasting group (Hydrologic Research Center) and a reservoir decision-support group (Georgia Water Resources Institute). This report focuses on the work of the forecasting group.

The primary tool for quantifying benefits is an integrated numerical system which involves components for ingesting and downscaling Global Climate Model (GCM) forecasts; generating ensemble reservoir inflow forecasts conditioned on downscaled GCM information; generating trade-off surfaces for decision support of multi-objective reservoir operation taking into consideration reservoir inflow uncertainty; and quantifying reservoir operation benefits for given release policies. The approach was introduced by Georgakakos et al. (1998) to assess the utility of climate model forecasts for operational water resources management. In the present

study, two watersheds in the Southeastern United States are examined. For the Lake Lanier watershed in Georgia, the historical period of analysis is 1949-1995. The second watershed is the Lake Norris basin in Tennessee and Virginia, which was modeled for the period 1949-1990. In each watershed, hydrologic models were applied, calibrated, used to generate inflow forecasts to the reservoirs over each historical period. These forecasts were then passed to the decision support group to be ingested by the reservoir model.

This work presents an intercomparison of the forecasting results using ensemble forecasting with uncertainty (ESP modeling), and with the ensemble forecasting conditioned on two different GCMs. The first model is the coupled CGCM1 model of the Canadian Centre for Climate Modeling and Analysis. The second is the ECHAM3 model developed at the Max Planck Institute for the European Centre for Medium-Range Water Forecasts. A vital difference for this application is that the CGCM1 model consists of a single realization or run, while for the ECHAM3 model, an ensemble of 10 model realizations is available. Thus, the multiple realizations offer a variety of conditioning possibilities, which must be combined to illustrate the use of this type of GCM.

Principal findings show that for these basins, there is little correlation between the monthly GCM forecasts in the region and the monthly-averaged basin precipitation. As such, the climate forecasts provide little information that can be used in improving forecasts over the traditional ESP forecasting methodology. The work does illustrate the use of ensemble GCM forecasts versus single GCM forecast. Finally for these basins, some improvement in the reliability of forecasting reservoir inflow volume for longer durations is shown.

This report is organized to provide the methodology and implementation in the following section. The focus watersheds are described in section 3, along with summaries of the of the hydrologic model calibration results. This is followed by a discussion of the relationship between GCM-scale and basin-scale precipitation, and then of the results and characteristics findings of the ensemble reservoir inflow forecasts.

2. Methodology

The framework for utilizing GCM forecast within the integrated forecast-control system is illustrated in Figure 1. Components of the system (shown in the figure by boxes) include models of global climate, catchment hydrology, and decision support for operational or planning management of reservoirs. The links between system components are provided through the downscaling of GCM forecasts and the generation of ensemble reservoir-inflow forecasts. An important feature in this system is the explicit accounting and forward propagation of forecast uncertainty throughout the system.

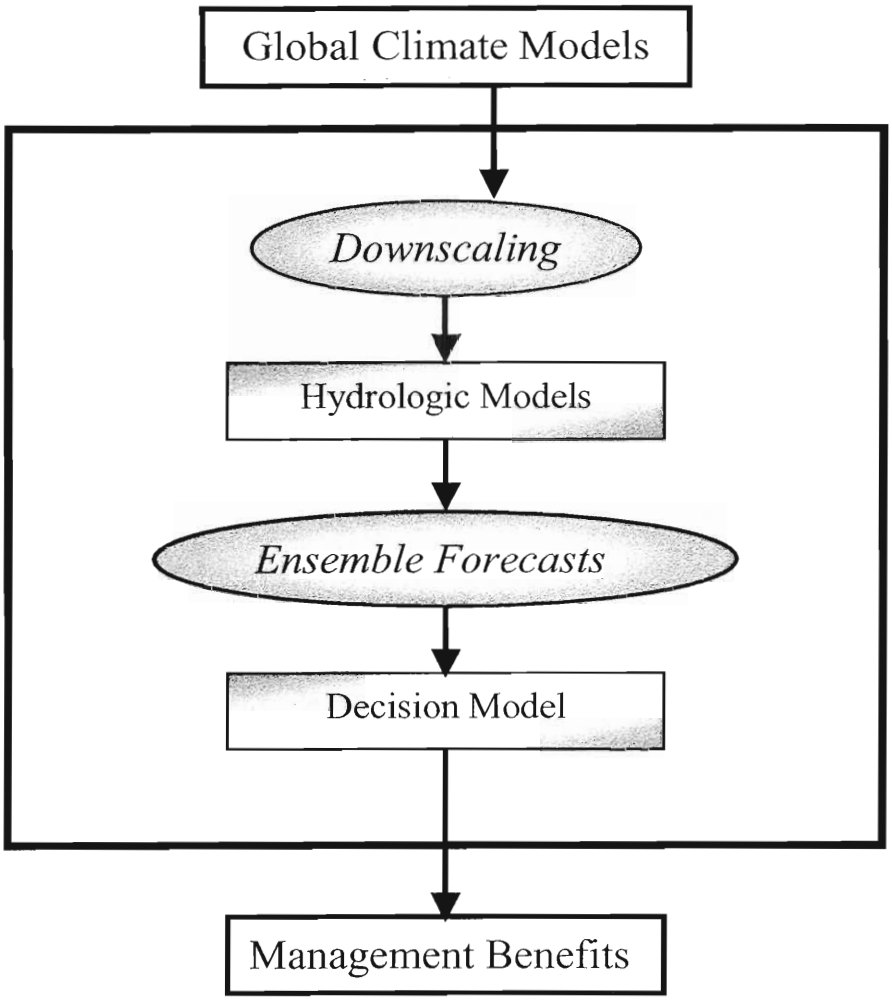

Figure 1. Illustration of integrated model methodology.

The reservoir releases identified by the reservoir decision support system are quantified in terms of specific reservoir management objectives, at varying forecast time scales and reliability levels. These objectives are specified through collaboration with various federal and state agencies with interests in the reservoir.

This system was first successfully applied by Georgakakos et al (1998) for the Upper Des Moines River basin in Minnesota and Iowa. Their work showed that when compared to

operational practices and to a forecast-control system that did not use climate information, this integrated system provided improved management benefits in terms of reductions in maximum daily flood damage, annual flood damage and spillage. Also the recent work of Carpenter and Georgakakos (2000) and Yao and Georgakakos (2000) presents the application of this system for Folsom Lake in the mountainous region of Central California. Their application is a comparison between a simple regression model, which does not account for forecast uncertainty nor makes use of climate information, and the forecast-control model used both with and without the benefit of climate forecasts. Again, the integrated system provides benefits over the simple regression model and over the system without climate forecasts.

The following sections describe the model components as applied for the current study watersheds.

2.1 GCM Forecasts

There are several global climate models run at various centers throughout the world. GCM models simulate the circulation of the atmosphere in three dimensions and produce estimates or forecasts of various atmospheric variables, such as temperature, pressure, and precipitation. Typically, sea surface temperature (SST) is prescribed and a set of ensemble forecasts is produced for different initial conditions. Recently, however, coupled ocean-atmosphere models have been developed which are not based on prescribed SSTs. These models are linked with ocean circulation models and thus the interaction and feedbacks between the atmosphere and ocean simulated. Both types of GCMs are utilized in this work.

The CGCM1 model of the Canadian Centre for Climate Modeling (ref) is a coupled GCM. This model was identified as a leading performer in climate systems simulations and was used in the U.S. National Climate Change Assessment (Hengeveld, 2000). The model grid spacing is approximately 3.75^{o} x 3.75^{o} in latitude and longitude (about 400 km). Secondly, the ECHAM3 model, development at the Max Plank Institute is also used. This model has a grid resolution of approximately 2.8^{o}. In contrast to the CGCM1 model, which consists of a single realization for the historic period, a set of 10 ensemble forecasts were available for the ECHAM3

model, based on varying initial conditions. For both GCMs, the variable extracted from the datasets is monthly precipitation.

Given the scale of GCM forecasts, an important issue is whether the GCM can reproduce observed conditions for the historic period. The Atmospheric Model Intercomparison Project (AMIP) and Coupled Model Intercomparison Project (CMIP) are two large, international studies that looked at the performance of different GCM models (Gates, 1992a; Meehl et al, 1997). In terms of water resources, paramount is whether the GCM provides some useful signal that can used advantageously in producing reliable flow forecasts. Thus, there is an assumption that some correlation between the GCM precipitation and the observed precipitation of the local basin exists. Even in the case of fairly low correlation between monthly averaged basin MAP and GCM precipitation (cross-correlation of approximately 0.4), Carpenter and Georgakakos (2000) demonstrate some improvement in reservoir inflow-forecasts with the use of climate information.

2.2 Downscaling

In this section, the issue is the downscaling of the monthly GCM data to the scale of observations for the basin, and the temporal resolution needed by the hydrologic model, e.g., daily data in the present studies. Following the work of Georgakakos et al (1998), a statistical downscaling methodology is used to relate the large-scale GCM forecasts (on the order of 100,000 km^2) to the much smaller scale of the watersheds of interest (on the order of a few 1000 km^2). Busiouc et al (1999), working with the ECHAM3 model, suggest that statistical downscaling produced reasonable results for seasonal precipitation in Romania. This is also supported by Sailor and Li (1999) for several sites in the U.S. for GCM-forecast versus local temperature.

Again, this approach is based on the assumption that the GCM has some correlation to observed precipitation and that information can be used to condition the input to the hydrologic model. For convenience, the monthly precipitation of the GCM node with highest correlation to the observed data is represented by P_i. The standardized anomalies of all P_i are computed over the historical period of the GCM, and then ranked to determined the anomaly values representing

the upper and lower tercile breakpoints of the distribution. Monthly anomalies within the same tercile (upper, lower, and middle) are used to condition the input of the hydrologic model. These inputs (precipitation and potential evaporation) are grouped by month and year based on the monthly GCM anomalies falling within the same tercile for the historical period. These groupings are used when generating the ensemble forecasts from the hydrologic model.

2.3 Ensemble Hydrologic Forecasts

The hydrologic model used in these studies is an adaptation of the National Weather Service (NWS) operational Sacramento soil moisture accounting model (Georgakakos, 1986). Input consists of precipitation (or rain + snowmelt) and potential evaporation, and the model produces estimates of total basin runoff at the catchment outlet. The model includes a set of parameters that require estimation. The calibration of the model for the two study watersheds is summarized in Section 3.

The ensemble streamflow prediction (ESP) methodology is used to produce a series or traces of likely flow forecasts for each basin. The approach used follows the operational NWS system (Day, 1985). ESP is based on the assumption that past atmospheric forcing is likely in the future, or that any past year is equally representative of future hydroclimatic conditions. In application, the hydrologic model is forced with observed precipitation and potential evapotranspiration up to the time of forecast to obtain estimates of the current soil moisture states. The model is then integrated forward in time using these states as initial conditions and using the historical record to drive the hydrologic model, each historic year in turn and starting from the same month and day as the forecast time. Thus, a set of equally likely flow prediction traces is generated over the forecast horizon. With a set of flow traces rather than a single forecast, the ensemble approach provides not only an estimate of future conditions, but gives a range of possible conditions, thus defining the uncertainty of the forecasts.

The set of ensemble forecasts are input to the reservoir control system. Based on the forecasts and their associated uncertainty, the reservoir model produces a set of optimal trade-off surfaces based on the operational policies and objectives of the reservoirs. From these trade-off surfaces, the cost of a given operational plan can be quantified.

Alternatively to the traditional ESP approach, in this application the GCM forecasts are used to precondition the use of certain historical years in generating the ensemble of inflow forecasts. Each monthly forecast of the GCM has been classified by the tercile of the GCM distribution within which they fall (see Section 2.2). For a given forecast date, the tercile of the GCM forecast for that date (month and year) is identified. For the generation of ensemble forecasts, the historical record for only those years for which the GCM forecast is in the same tercile as that of the forecast data is used to drive the hydrologic model. Thus, the ensembles are conditioned to favor those years that the GCM identifies as "similar".

In this work, three sets of ensemble forecasts were generated: (a) a set following the traditional ESP method where all historical years are used (termed "Baseline ESP" in the results section); (b) a set where the CGCM1 model data was used to condition the choice of historic years; and (c) a set where the years were conditioned on the ECHAM3 model forecasts. In each case, daily forecasts were made for the historical period with a forecast horizon of 120 days. As a retrospective study, all years of the historical record, less the year of the forecast, were used in generating the ensemble of inflow forecasts.

As the GCM-conditioned ensembles are produced from a subset of historical years, these have a fewer number of traces in each forecast than in the baseline ESP ensembles. To make comparisons between the different sets of forecasts, an equal number of traces in each case is necessary. This is accomplished by re-sampling from the historical years with an added random error until the desired total number of forecast traces is reached. The error is derived from the parameterization of the hydrologic model. After the hydrologic model is calibrated, there remains a residual error between the simulated flows and observed flows. The characteristics of this residual error are quantified in terms of a mean and standard deviation on a monthly basis, which is used to generate the parameterization error for each forecast trace and for each forecast made. The residual error characteristics are illustrated for the two study watersheds in Section 3. The error is added in each set of ensemble forecasts produced (baseline and both GCM-conditioned runs). The total number of forecast traces for each forecast is based on the number of traces for the baseline ESP run and is equal to the number of historical years less one for the year of the forecast date.

For the ECHAM3 data, 10 sets of forecasts were generated; one from each ECHAM3 realization. To condense these sets into one that encompasses the results of the individual ECHAM realizations, the sets were combined by extracting from each set an equal number subset of forecast traces for each forecast date.

2.4 Validation of the Ensemble Forecasts

Reliability diagrams provide the primary validation tool for the ensemble reservoir inflow forecasts. The diagrams illustrate how well the forecast frequency of a given occurrence (i.e., flow volumes in the upper tercile of the distribution) matches that of the observed frequency. To start, the upper and lower tercile bounds of the observed flow volume were determined for durations of 30-, 60-, 90-, and 120-days. The reliability diagrams are then developed as follows. First, for each forecast date, the N-day forecast volume for each ensemble trace is compared to the observed volume bound for the same duration. The fraction of ensemble forecasts that meet the criteria of being greater or equal to the upper tercile bound is computed. This is the forecast frequency for the event meeting the given criteria (i.e., flow volume in the upper tercile). Thus, if the forecast frequency meeting this criteria for given forecast date is 90%, it is said that the model is confident of the flow volume being in the upper tercile for that date. This is done likewise for the criteria of the forecasted flow volumes being less than or equal to the lower tercile bound. After all forecast dates are processed, the forecast frequency, with a range of 0 to 1, is divided into 10 equal interval bins. For each bin, the observed flow volumes for the dates of the forecast events within that bin were compared to the same volume bound for the given criteria (i.e., in the upper or lower tercile). The frequency of the observed flow volumes matching the criteria then computed for all forecast dates within each bin. Under a perfect forecast, the observed frequency would match the forecast frequency, and thus the expected observed frequency is equal to the midpoint of the forecast frequency bin. Large deviations from equality of observed frequency and forecast frequency indicate unreliable forecasts for that interval of forecast frequency. The reliability diagrams were produced for flow volume durations of 30-, 60-, 90- and 120-days and for both criteria of the upper tercile volumes and lower tercile volumes.

To quantify a "large deviation", confidence bounds for each frequency subinterval are defined under the assumption that the probability of a given observed inflow volume falling within that subinterval is fixed and equal to the interval midpoint. Under this assumption (e.g., Benjamin and Cornell, 1970), the number of observations ("forecast events") in a given forecast frequency subinterval, N_I, has a binomial distribution with an expected value $N_S p$ and variance $N_S p\ (1\text{-}p)$. N_S is the number of observed inflow volume samples within the bin and p is the constant probability of observed a certain sample. Then, a standard residual, v, is defined as:

$$v = \frac{N_I - N_S p}{\sqrt{N_S p(1-p)}} .$$

This standard residual is included on the reliability diagrams as an error bar from the expected frequency. For frequencies outside the errors bars, the forecasts are unreliable for that subinterval of forecast frequency. In cases where N_I or N_S is too small (i.e., less than 25), the reliability and standard residual are not computed.

In addition to the reliability diagrams, a Brier score (reference?) is also computed for each duration (30-, 60-, 90-, and 120-day volumes) and for the upper and lower tercile criteria. This score is computed as:

$$B = \sqrt{\sum \frac{N_I}{N_{tot}} (f_{\exp I} - f_{obsI})^2} ,$$

where N_I = the number of forecasts events in the given subinterval;

N_{tot} = the sum of N_I in all subintervals;

f_{expI} = the expected observed frequency for the given subinterval;

and f_{obsI} = the actual observed frequency for the given subinterval.

Thus the Brier score is a weighted measure of the total distance of the observed frequency from the expected frequency for all forecast frequency subintervals. A small Brier indicates a smaller deviation from the expected frequency. Characteristic reliability and Brier score diagrams are presented in Section 5 for the two study watersheds.

3. Application Basins

Lake Sydney Lanier is located in the northern Georgia, as shown in Figure 2, with a contributing drainage area of nearly 2700 km^2. The reservoir is operated by the U.S. Army Corps of Engineers (USACE) with objectives of flood control, power production, navigation, water supply, recreation and wildlife management. There are two main tributaries into the lake, the Chestatee River and the Chattahoochee River. Figure 2 shows relevant hydrometerologic reporting stations, along with the period of observed data. Due to the available record, initial calibration of the hydrologic model was done for the Chattahoochee River near Cornelia (drainage area of 806 km^2) and for the period 1948-1995. The simulated flows were then scaled based on area alone to the Gainesville location, and to the total reservoir drainage area and compared to the available data that these locations. An accounting of the difference in total volume of inflow (simulated) and total volume of outflow (observations of downstream flows at Buford Dam) showed a continuous and substantial accumulation of volume since the reservoir went into operation in 1958. Thus, scaling of the calibrated model flows at Cornelia to the full drainage area was not adequate (Carpenter & Georgakakos, 1999, also noted the dependence of Sacramento model parameters to scale of basin.). Thus a three-subbasin model was developed to include: the Chattahoochee River basin at Gainesville, which accounts for over one half of the total drainage area; the Chestatee River basin at Dahlonega, which contributes 390 km^2 to the drainage area; and the local drainage to the reservoir accounting for the final 840 km^2 of the drainage area. Mean areal precipitation (MAP) forcing was derived for each subbasin, and regional potential evapotranspiration (PET) forcing was used. The hydrologic model parameters from the Cornelia calibration were applied to the three subbasins; then adjusted based on the available record for those locations. The outflow of the three subbasins is added to provide the inflow to the reservoir. Thus, this assumes that the travel time from the subbasin outlet to the reservoir is within the time step of the simulation, or 1 day. A dataset of unimpaired inflows for Lake Lanier were supplied by USACE and used as observed flows for the comparison with the simulated total inflow. Table 1 provides statistical summaries of the simulations. The simulation of inflows into the reservoir covered the period 1948-1995.

Figure 3 shows the annual cycles of basin MAP and PET, observed flows, and simulated flows for Lake Lanier. The average monthly variation of precipitation for the basin is not significant. There is a small peak in March and another in July, with an overall range in average monthly MAP from 3.4 to 5.5 mm/day. The reproduction of the annual flow cycle by the model is quite good. In the Figure, the observed flows are represented by the unimpaired flow data as obtained from USACE. During the fall (August through October), the model tends to over-simulate the observed flows, followed by a slight under simulation in winter (November through January). This residual is also shown in the Figure (part b). The error bars give the 1-standard deviation bounds of the daily residual error. The average residual from the simulation is small, although the variation in daily residual can be large. The characteristic parameterization errors were developed from these monthly residual statistics, sampled and added to the ensemble flow forecasts as described in Section 2.3.

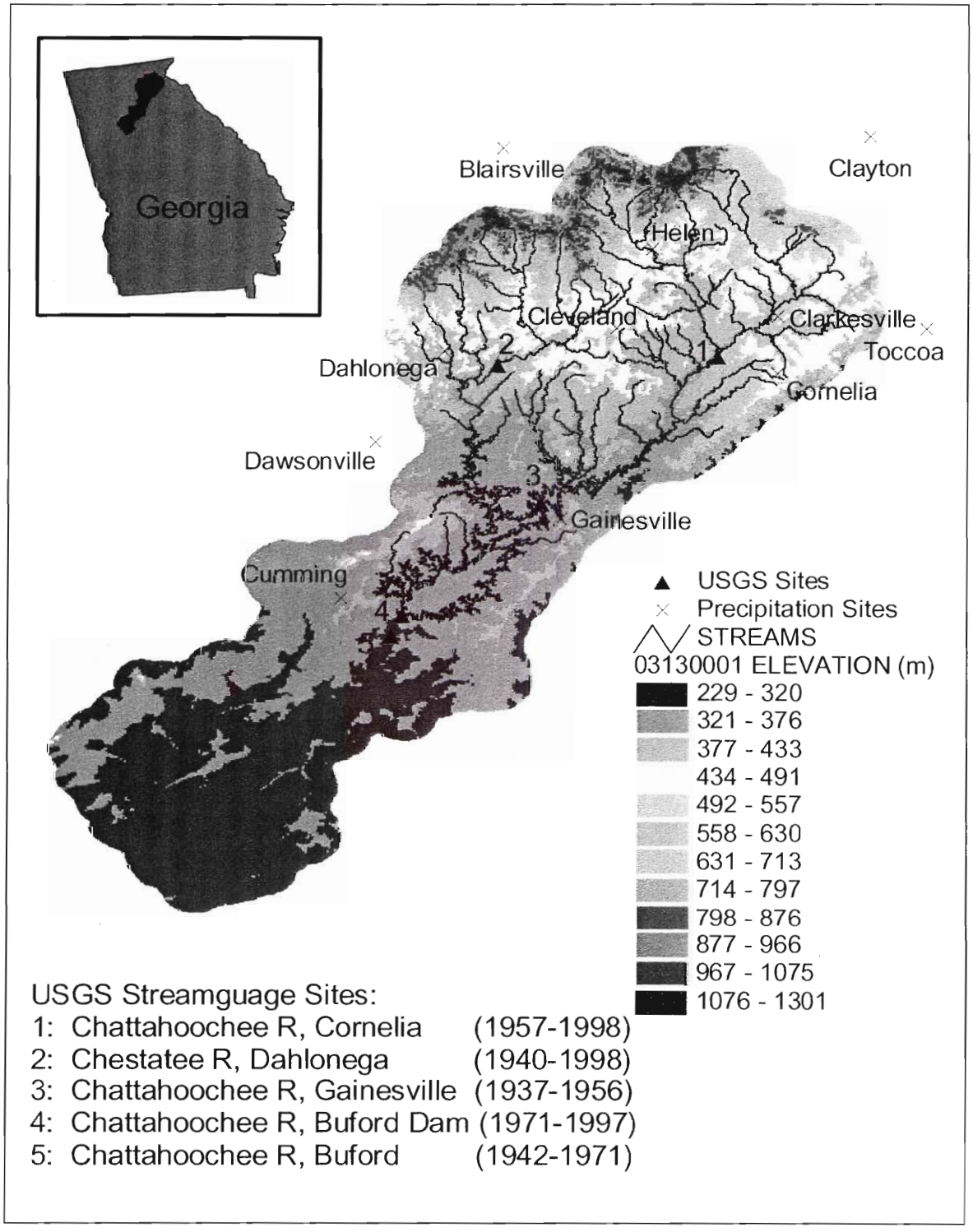

Figure 2. Location of the Lake Sydney Lanier watershed, part of hydrologic unit #03130001. Included in figure are locations of streamflow and precipitation gauges.

Table 1. Summary of Residuals for Calibration sites

	Average Residual	Standard Deviation	Cross-Correlation
Lake Lanier:			
Chattahoochee R, Cornelia	125.8	364.2	0.87
Chattahoochee R, Gainesville	204.6	678.6	0.86
Chestatee R, Dahlonega	31.55	204.8	0.86
Inflow to Lake*	35.13	717.0	0.91
Lake Norris:			
Clinch R, Tazwell	6.60	1240	0.93
Powell R, Arthur	44.08	697.8	0.93

* For this comparison, simulated flow was processed with 7-day smoothing filter to match USACE unimpaired flows, thus yielding higher cross-correlation.

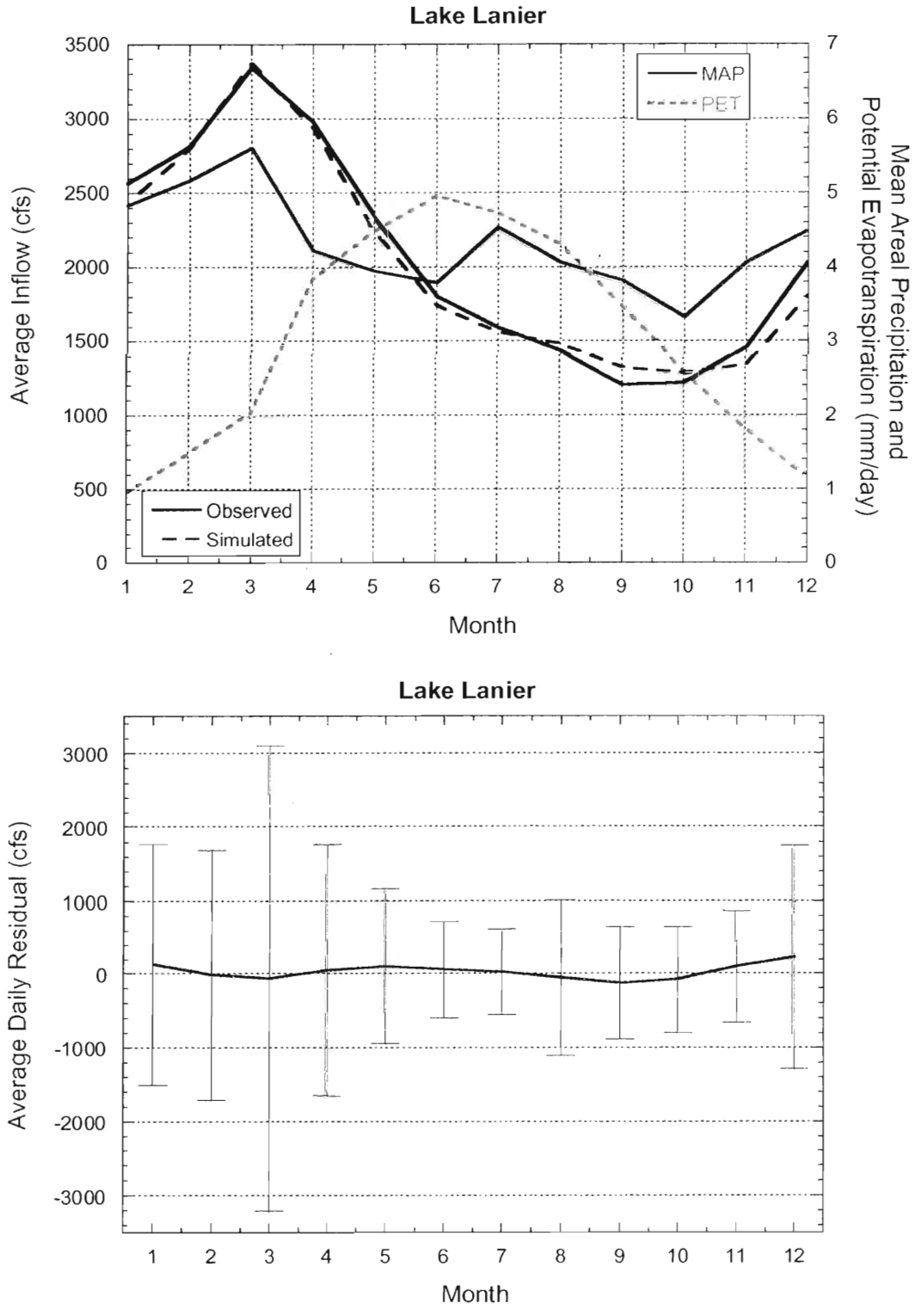

Figure 3. Calibration of the hydrologic model for Lake Lanier. Part (a) presents annual cycle of MAP, PET, and flow; (b) presents average simulation error.

The Clinch and Powell Rivers drain parts of Western Virginia and Tennessee and provide the inflows into Lake Norris in northern Tennessee (see Figure 4). The basin is located between the Great Smokey Mountains on the East and the Cumberland Plateau to the West. Also shown in Figure 4 is the location of relevant hydrometeorologic stations. The two rivers exhibit varying runoff-response in terms of response timing and yield. Therefore, the hydrologic model was calibrated for two subbasins: the Clinch River above Tazwell, TN; and the Powell River near Arthur, TN. These two subbasins, with a combined drainage area of 5590 km^2, account for approximately 75% of the total drainage area of the Clinch River below Lake Norris. As these are the major gauged inflow locations, their sum was taken as the total inflow to the reservoir. Results of the calibration for the two subbasins are presented in Table 1 along with the Lake Lanier statistics. The correlation of the simulated flows for the two subbasins is very good. The reservoir inflow was simulated for the period 1949-1990. The annual cycles of basin MAP, PET, observed flow, and simulated flow are shown in Figure 5. January through June precipitation has a nearly constant value of 3.5 mm/day. The "peak" MAP of 4.0 mm/day is observed in July, followed by a steady decline to the low of 2.5 mm/day in October. The simulation of flows is still quite good. The observed flows are over- simulated in January and February, followed by a slight under simulation through the spring and summer. The average daily residual errors are also shown in the Figure (part b), with the error bars representing the 1-standard deviation bounds of daily error. The maximum average residual error of approximately 500 cfs occurs in February, with relatively large variability seen for most months. Again, these residual statistics were sampled as characteristic parameter error in the generation of ensemble forecasts.

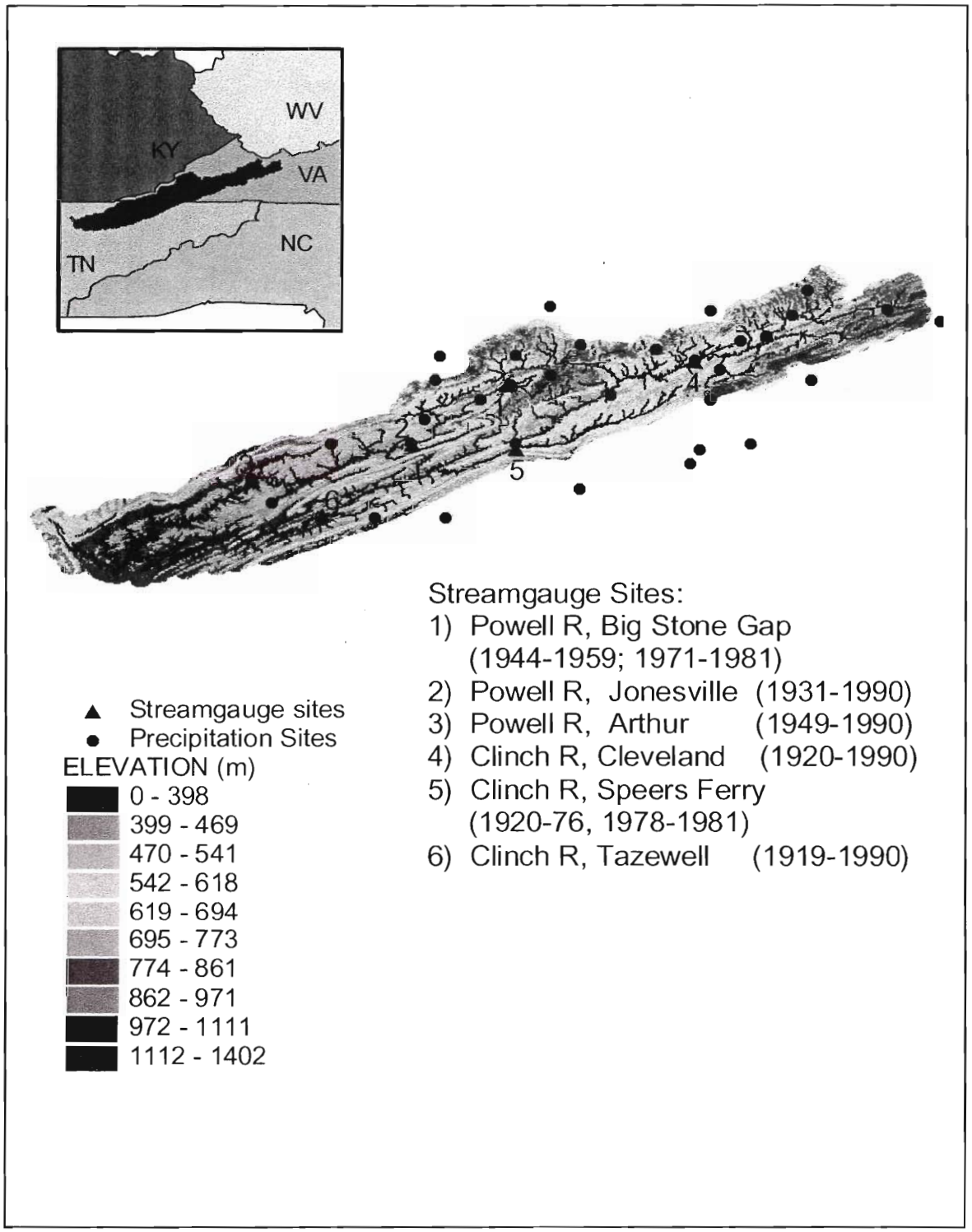

Figure 4. Location of Lake Norris watershed with streamflow and precipitation gauges indicated.

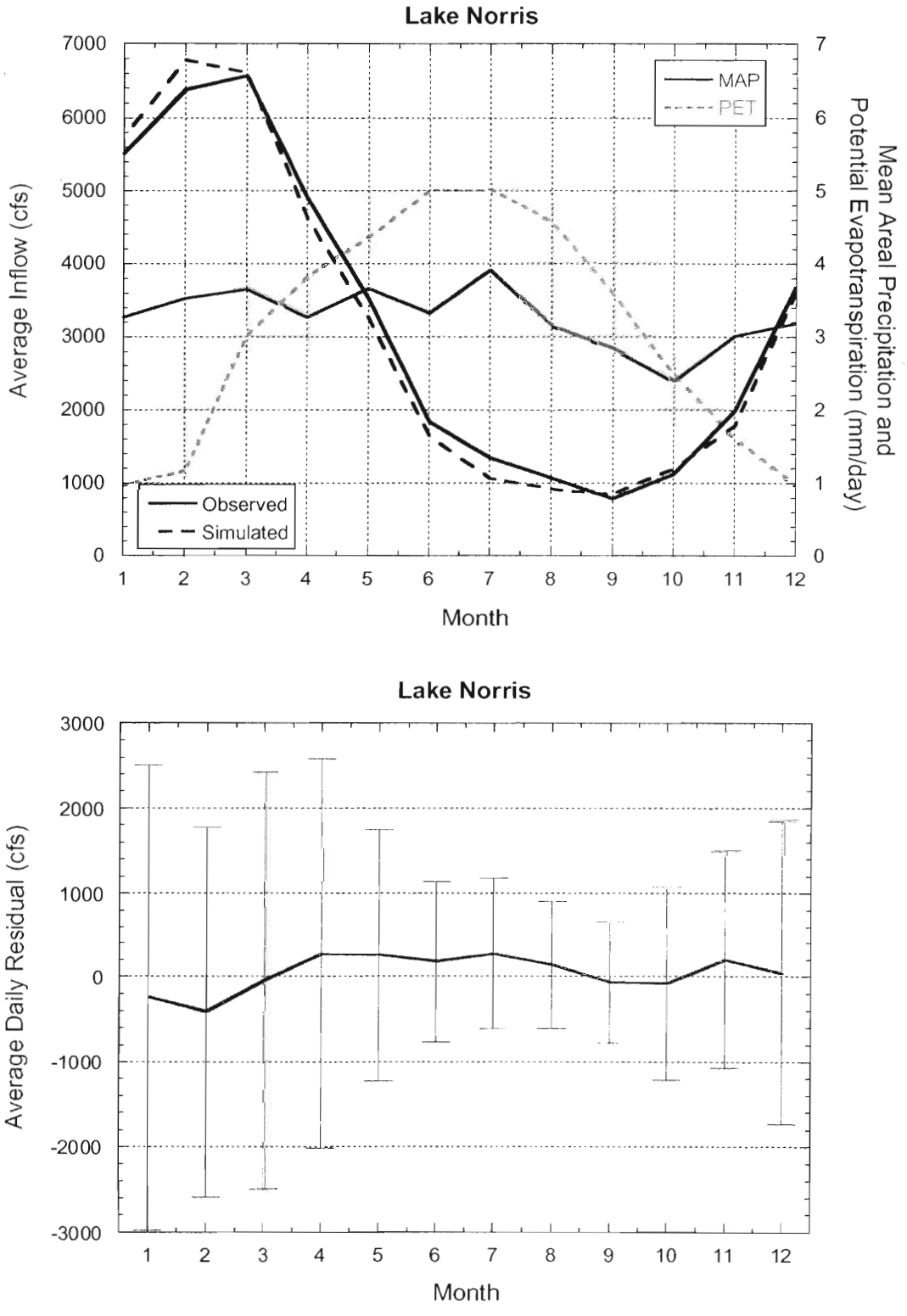

Figure 5. As in Figure 3 for the Lake Norris watershed.

4. GCM Downscaling at Application Basins

Paramount in the methodology is the association or relationship of the large-scale GCM data, covering areas of approximately 3° x 3°, to the scale of the watersheds, which are generally on the order of a few thousand square kilometers. The GCM estimates must be related or downscaled to the input of the hydrologic model. Figure 6 shows the scale of the GCM to the two basins of this study. The solid circles represent the center of the 2.8° x 2.8° grids of the ECHAM3 data. The locations of the CGCM1 grid nodes are spaced slightly wider, although the vast scale difference is apparent with the ECHAM3 locations.

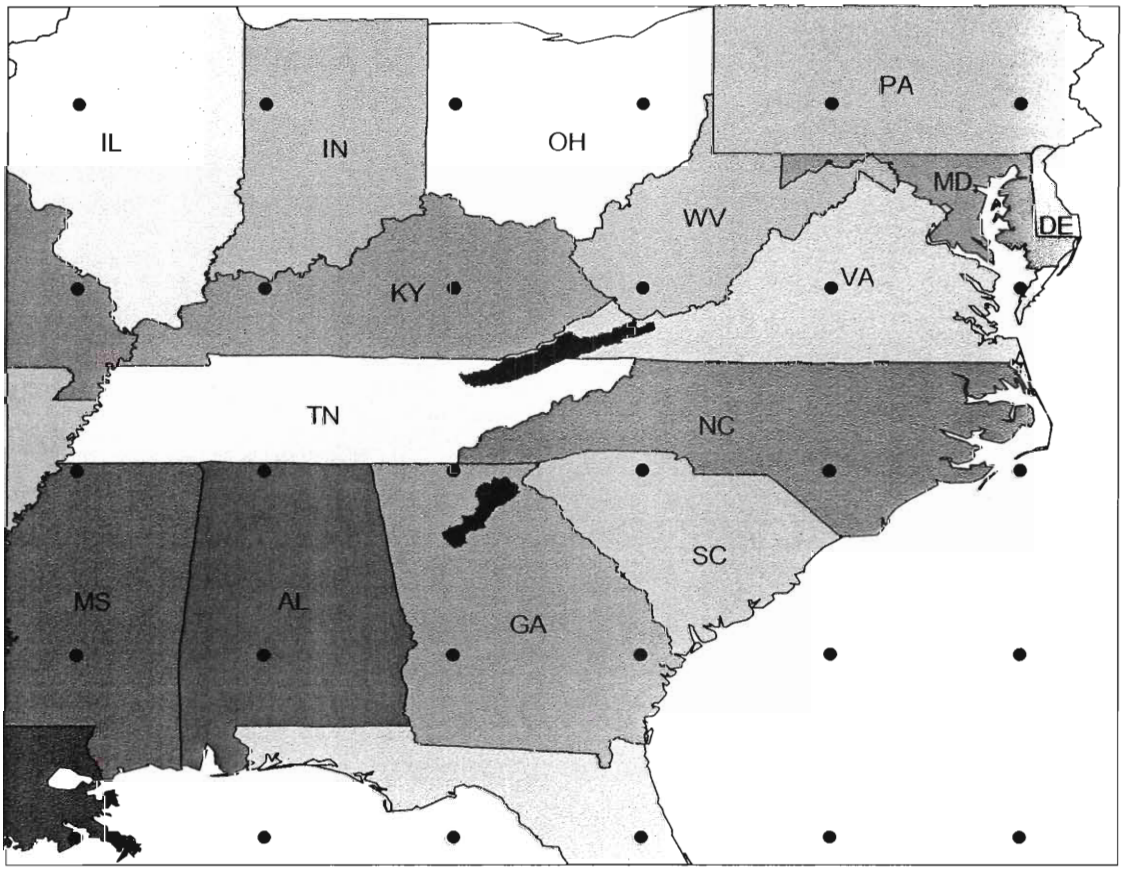

Figure 6. Scale of ECHAM3 GCM nodal points to study watersheds.

Monthly values of basin MAP for the two study locations were compared to the GCM precipitation for several GCM nodes nearby each basin. To illustrate the relationship between GCM and basin precipitation, the annual cycle of both are plotted in Figure 7a for Lake Lanier and with the six closest CGCM1 nodes. The basin MAP is shown with the thick black line, and the CGCM1 data are shown with varying colors. The annual cycle for the CGCM1 data is more amplified and delayed in time relative to the observed cycle. The GCM data generally shows a peak in April or May and second, often larger peak in September or October. In contrast, the peak of the observed is in March, with a trough in October. The correlations between the two monthly precipitation estimates, also shown on the Figure, are nearly zero. Several variations were attempted in an effort to improve the correlation, from averaging multiple nodes to examining seasonal values of precipitation. However, this yielded no significant improvement in the correlation. For Lake Lanier, the CGCM1 node directly north of the watershed (labeled "67" in the plot) was selected, as it is the closest node to the watershed. Similarly, Figure 7b illustrates the annual cycles for the ECHAM3 case. For the ECHAM3 data, each node has a set of ten realizations of precipitation to examine. In the Figure, three ECHAM3 nodes are presented. These nodes were identified as the best possibilities from a set of 20 nodes surrounding the basin. For this case, the timing of the peaks in precipitation is much better, matching the spring and summer peaks of the observed MAP. For the ECHAM3 case, the far north grid node (labeled "147" in the figure) was chosen, as it appears to come closest to capturing the observed peak March followed by a smaller peak in July/August.

The relationship between GCM precipitation and basin MAP for Lake Norris tended to be show less correlation as there is little interannual variation in basin MAP. For Lake Norris, the GCM nodes in both CGCM1 and ECHAM3 cases were selected based on proximity to the basin. As final evidence regarding their relationship, the GCM precipitation is plotted against monthly-average basin MAP values for the selected nodes of each GCM in Figure 8. For the ECHAM3 data, only one of the 10 realizations is presented. The cross-correlation for the ECHAM3 realizations ranged from 0.08 to 0.18 for Lake Lanier, and from 0.02 to 0.16 for Lake Norris. Clearly, little correlation exists between the GCM and basin precipitation.

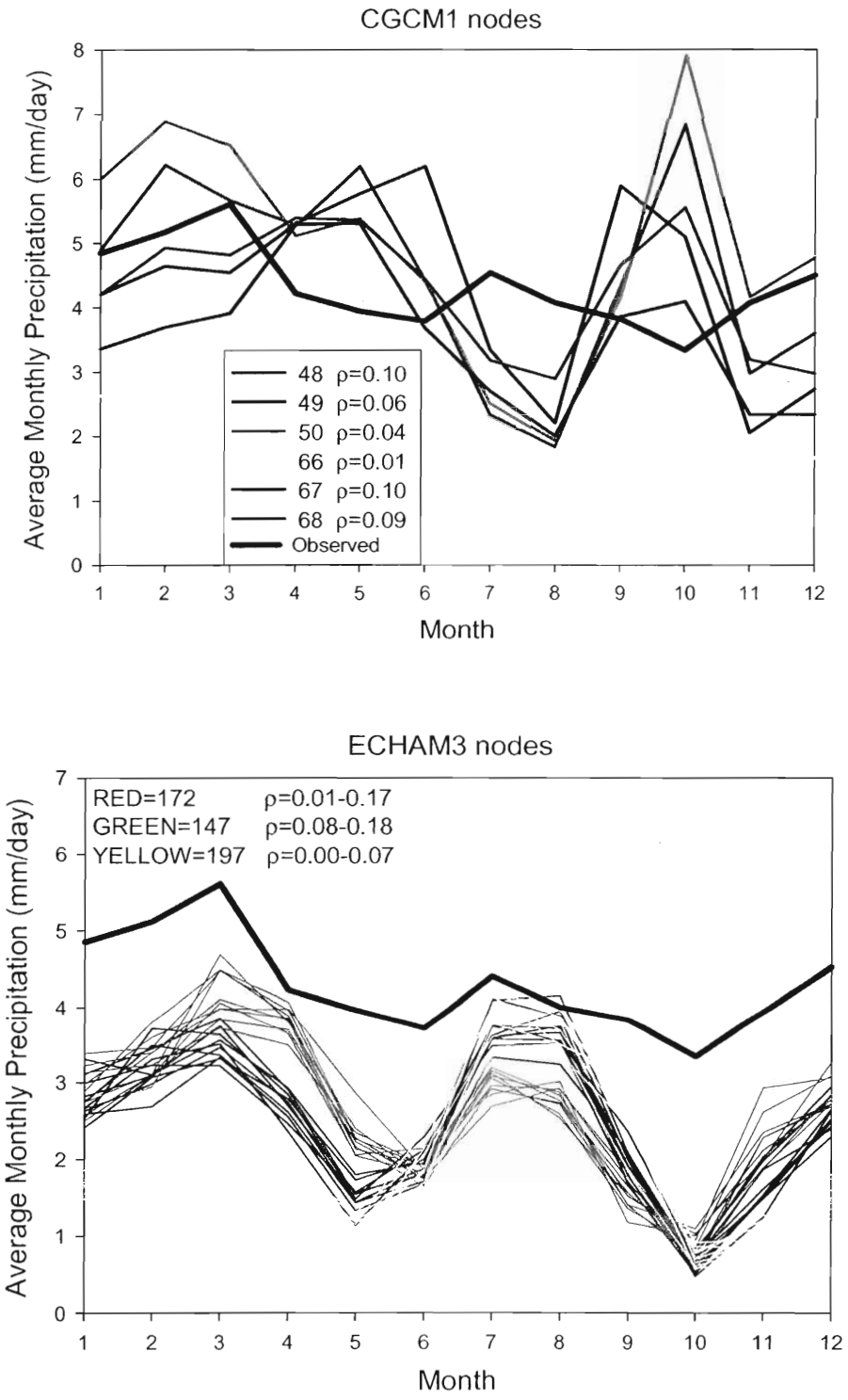

Figure 7. Annual cycles of GCM-precipitation and monthly averaged basin MAP for Lake Lanier and for selected GCM nodes.

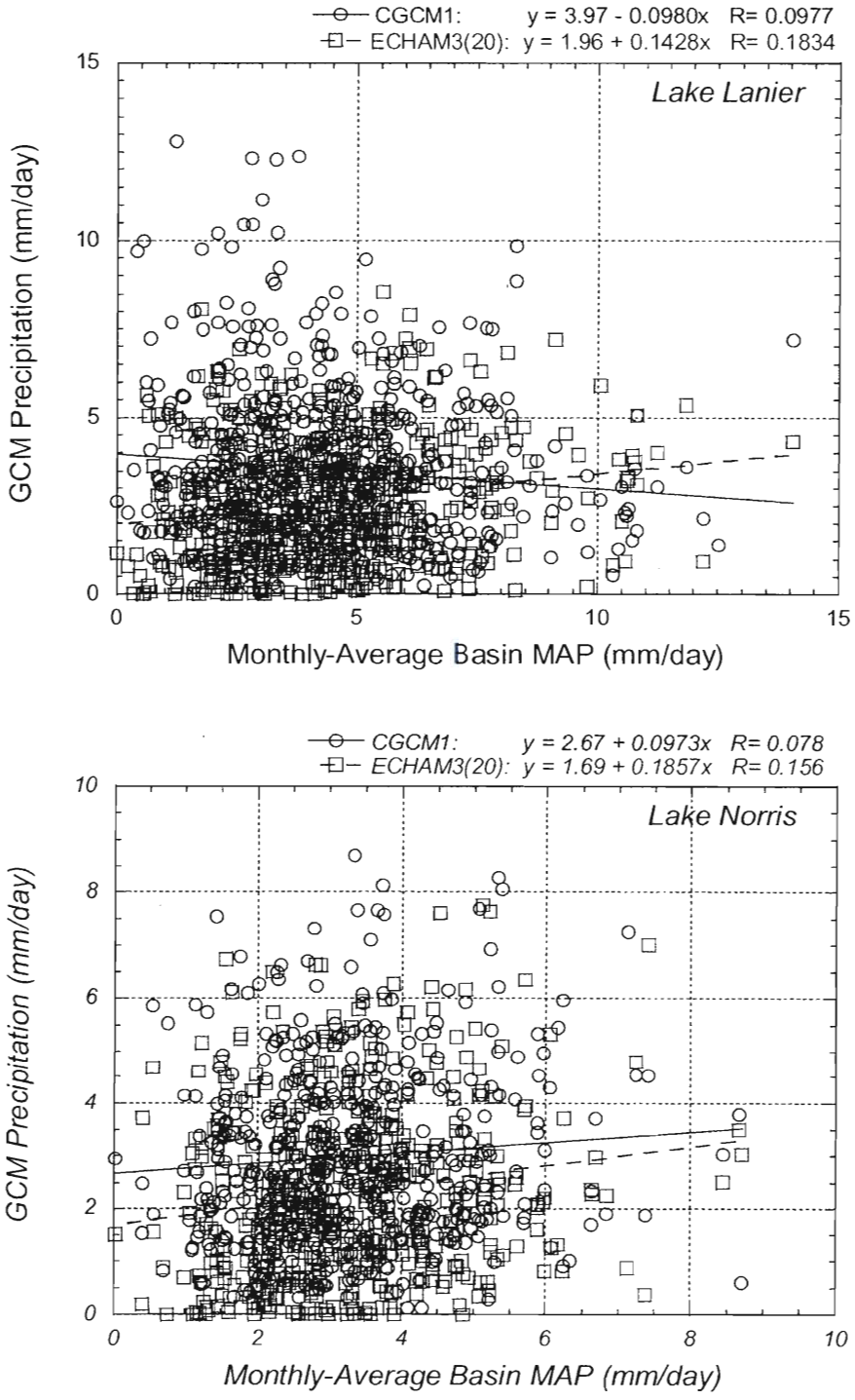

Figure 8. Association of monthly-averaged basin precipitation and GCM precipitation for the selected nodes of the CGCM1 and ECHAM3 GCMs. Only one ensemble of the ECHAM3 data is presented.

Ultimately, however, it is whether the GCM can supply some information that can be used to distinguish the input to the hydrologic model. To illustrate whether the division of the GCM data by tercile can distinguish any difference in the hydrologic model input, Figure 9 presents the cumulative frequency distribution of observed daily MAP for two cases: (a) periods when the GCM is in the upper tercile (green line) and (b) periods when the GCM is in the lower tercile (red line). Ideally, the two lines would be separate or diverge towards the tails of the distributions. As in Figure 8, only one plot from the possible 10 ensembles of the ECHAM3 data is presented.

For Lake Lanier, there is some separation of the frequency distributions for very extreme events (i.e., frequency > 90%). Use of the CGCM1 data shows a greater separation than when the ECHAM3 data, which shows a slight separation for frequency values greater than 95%. Of the ECHAM3 ensembles, one half result in at least a slight separation for the two cases. The other half show no discernable difference in the daily MAP whether the GCM data is in the upper or lower tercile of its distribution. For Lake Norris, there is no significant difference in the two distribution, except as shown in Figure 9, where in a few cases, there is some variation in the top 1% of the frequency distribution.

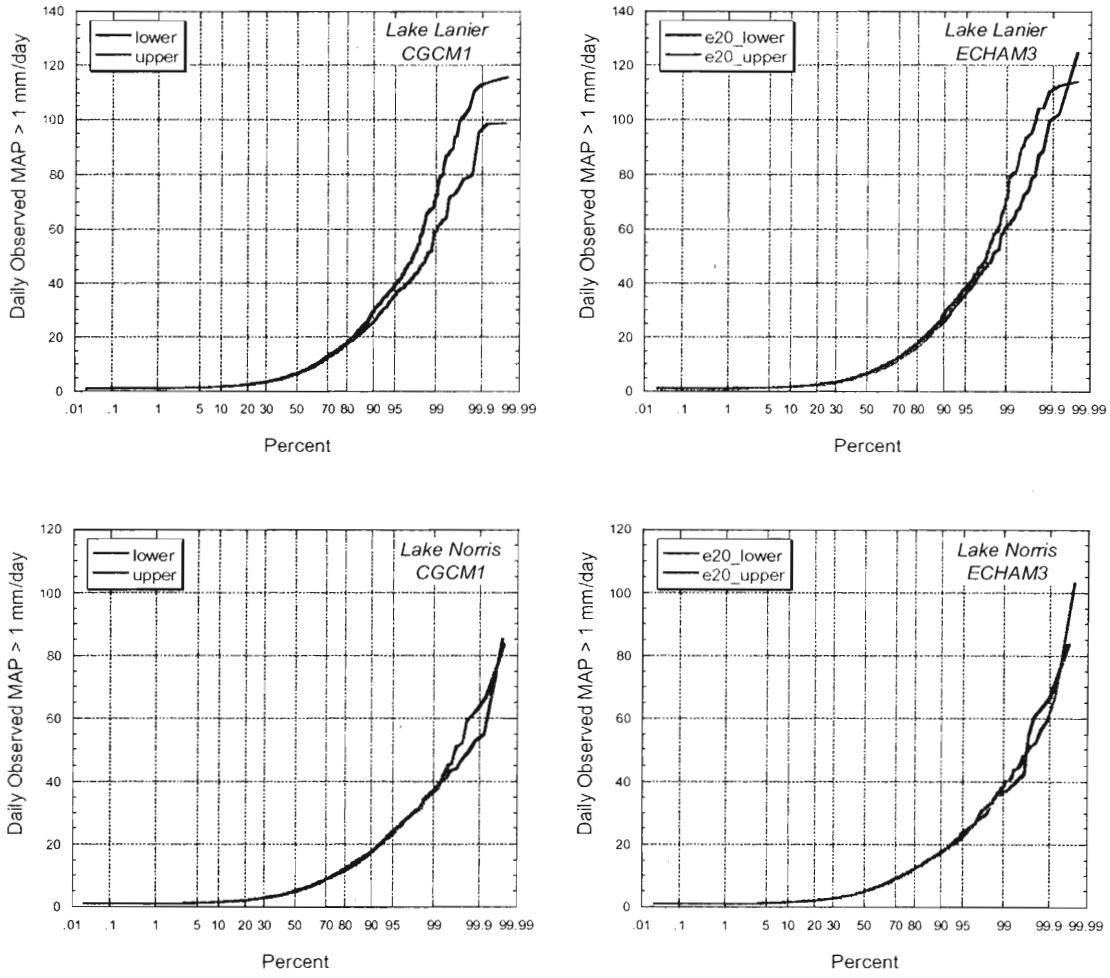

Figure 9. Cumulative frequency distributions of basin MAP when GCM is in extreme terciles. One plot is given for each watershed and for each GCM.

5. Ensemble Forecast Results

For each day in the historical period, the hydrologic models of the two watersheds were used to produce three sets of ensemble reservoir inflow forecasts with a forecast horizon of 120 days. Thus, more than 17,000 forecasts were produced over the historical period for Lake Lanier, and nearly 15,000 for Lake Norris. An illustration of the ensemble forecasts is presented in Figure 10 for an event in late March 1977 for the Lake Lanier basin. The figure shows the observed flow along with three sets of ensemble forecasts, on different forecast dates, for each of the three cases: baseline ESP; ESP conditioned on the CGCM1 data; and the combined ESP forecasts conditioned on the ECHAM3 data. All ensembles start from the simulated model states at the time of the forecast. Before the event occurs, most of the traces show little response as the other historical years did not show significant precipitation for the particular day (month and day) of the forecast date. Once the event is observed, the model states adjust and all forecast traces are significantly higher. After the event, model states again adjust to produce lower flows, with some chance of increased flows over the last few days appears in several traces.

When comparing the GCM-conditioned plots to the baseline ESP run for this event, little difference is noted. Generally, the mass of the GCM-conditioned traces, particularly for the ECHAM3 GCM, do not appear closer to the observed flow than the traces of the baseline ESP run. The range in flows for each GCM-conditioned case is similar to the baseline ESP run. However, there is less variability in the flow traces for the CGCM1-conditioned results.

To get an overall view of the accuracy of the ensemble forecasts, residual errors between the forecast and the observed flows were computed for each forecast trace and for each forecast date. The average is computed over all forecasts made. Also computed is the average observed flow over the same basis. Generally the errors are found to be fairly small. For Lake Lanier inflows, the errors are roughly centered about zero and are generally within +/- 500 cfs to 40-50 days into the forecast horizon. The thick black line shows the average of the average residuals computed over the traces. This average is quite small, less than 100 cfs over the entire forecast horizon for Lake Lanier forecasts.

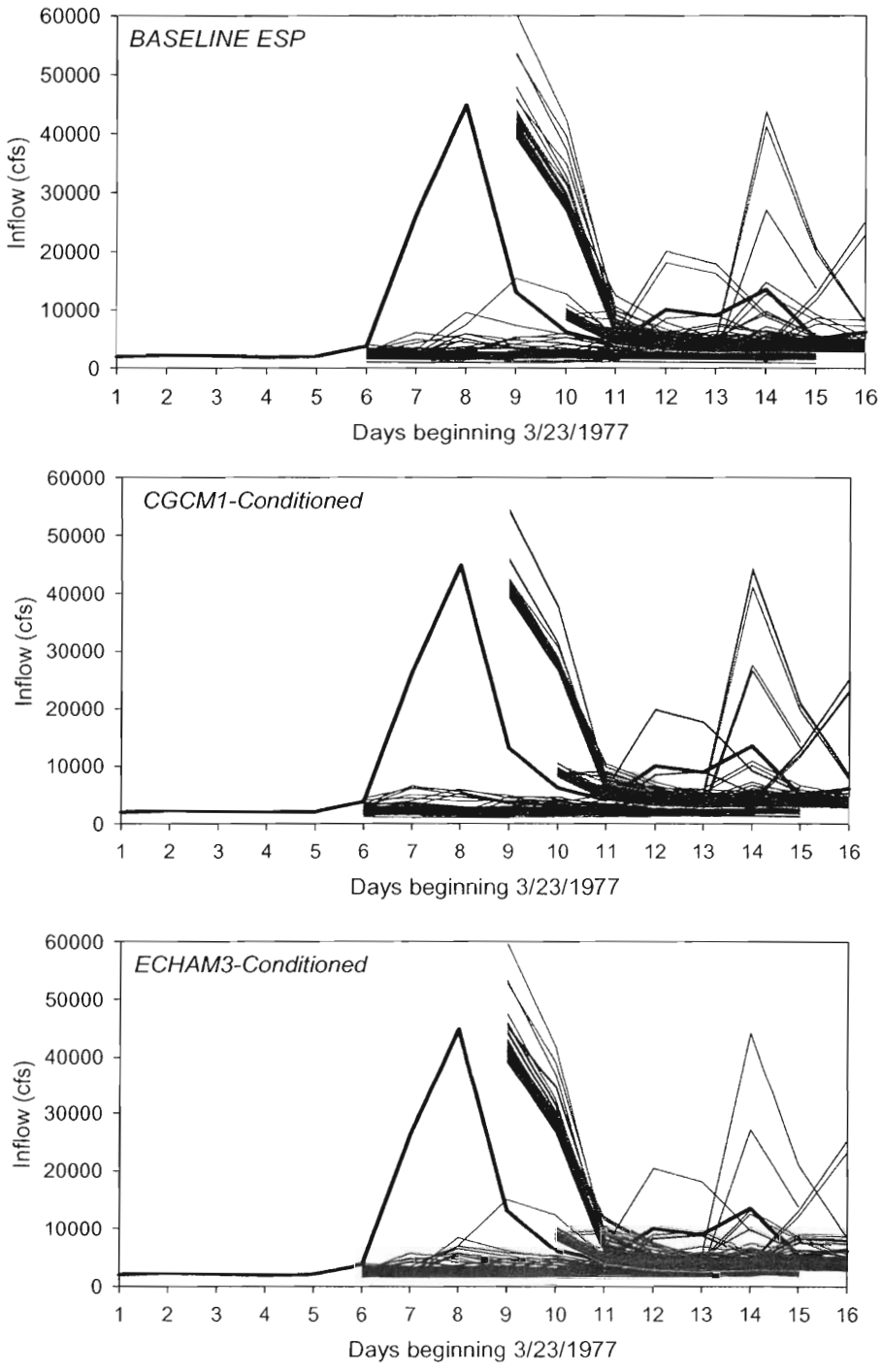

Figure 10. Illustration of ensemble forecasts for event of March 1977 for the Lake Lanier basin.

As the historical years are repeated as necessary to obtain the same number of traces as the baseline ESP run, the average residual by trace year was not computed for the GCM-

conditioned cases. However, the residual errors were averaged over both ensemble traces and forecast dates for the GCM-conditioned runs. This average for the three cases is shown in Figure 11 for Lake Lanier inflows. The dashed lines indicated the 1 standard deviation bounds of the average errors.

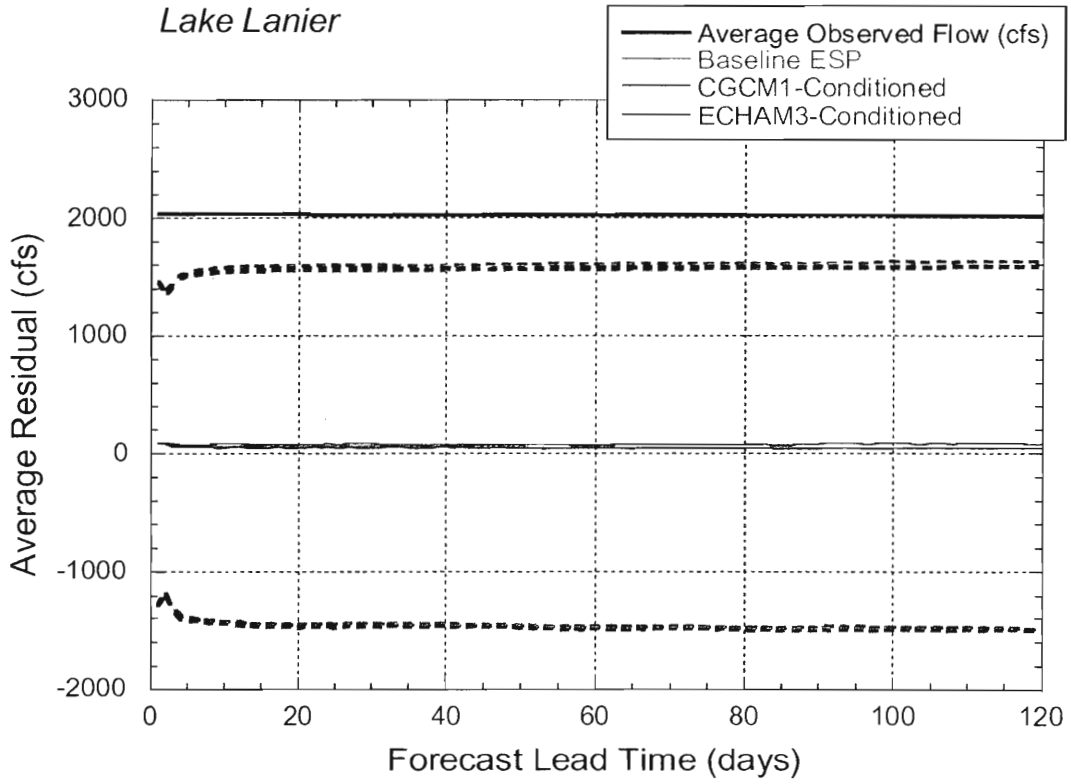

Figure 11. Average residual error of forecasts for forecast horizon of 120 days for Lake Lanier.

The residuals for the baseline ESP run are small and little difference can be seen for either case of GCM-conditioning.

As stated in Section 2.4, the primary tool for assessing the ensemble forecasts is the reliability diagram. These diagrams were produced for inflow volumes of 30-, 60-, 90-, and 120-day durations and for volumes in both the upper third and lower third of the observed

distribution. Figures 12 and 13 present the reliability diagrams for Lake Lanier and Lake Norris, respectively. Each figure shows the 30- and 120-day inflow volume diagrams for volumes in the upper tercile and the lower tercile. In each diagram, all three cases (baseline ESP, ensembles conditioned on CGCM1, and ensembles conditioned on ECHAM3) are included and represented by different symbols. The error bounds are described in Section 2.4 and those shown are the maximum allowed from the three cases, although these bounds did not vary significantly between the three cases. For the 30-day inflow volume for Lake Lanier, the forecasts become unreliable for forecast frequencies greater than approximately 0.6 for both volumes in the upper tercile and in the lower tercile. However, this deviation from the reliability error bounds appears to diminish as the duration of the volume forecast is increased to 120 days.

For Lake Norris, the 30-day inflow volume forecasts are reliable to forecast frequencies of approximately 0.5 for volumes in the lower tercile and to frequencies of 0.65 for volumes in the upper tercile. With the 120-day volumes, the number of forecasts within the upper forecast frequency range decreases, notably for the upper tercile case, and thus the reliability is not computed in this range. The reliability for the 120-day volume forecasts in lower frequency ranges is similar to those of the shorter duration volume forecasts.

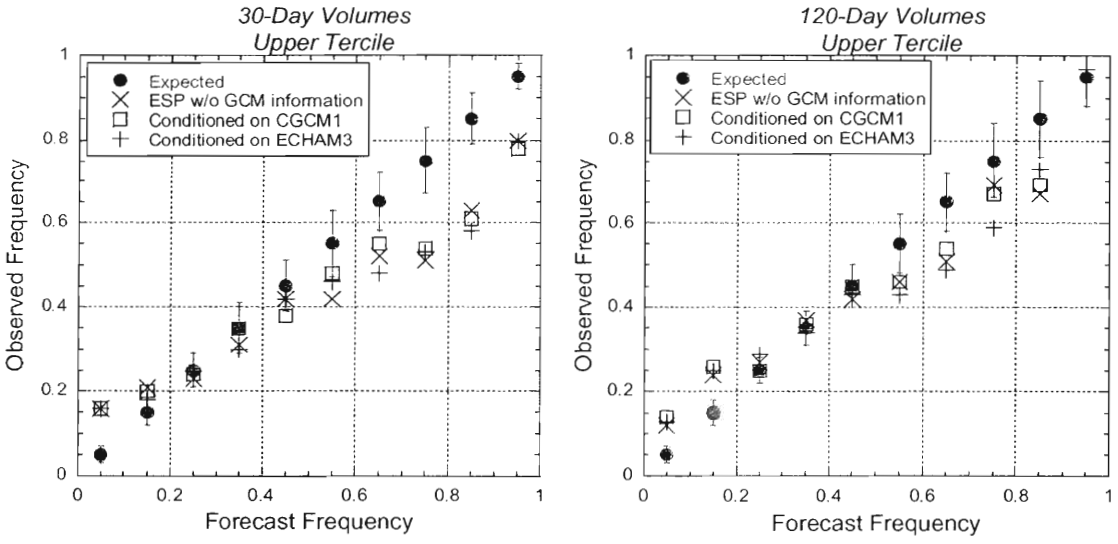

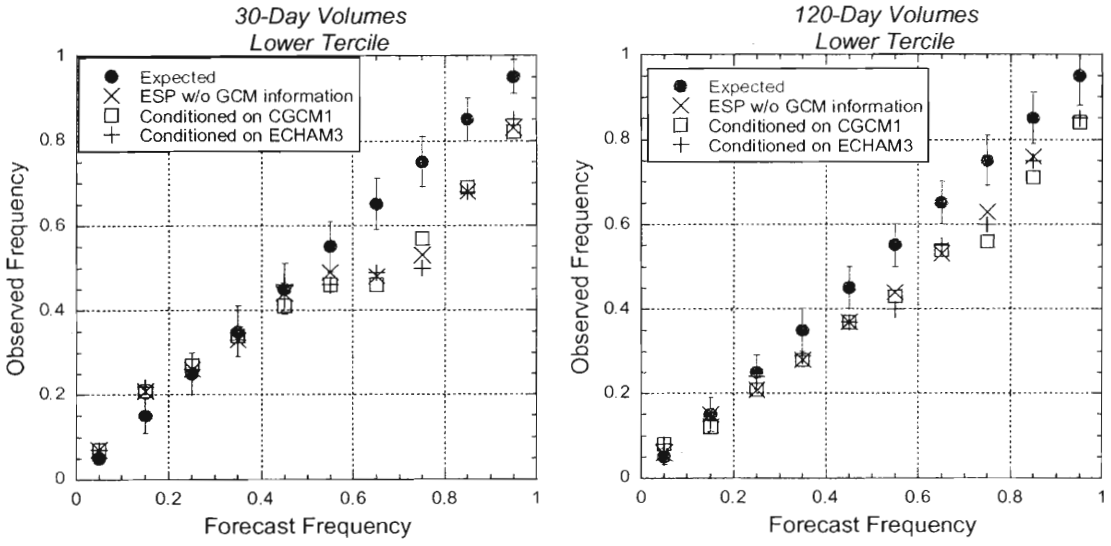

Figure 12. Reliability diagrams for Lake Lanier inflow volume forecasts of 30-day and 120-days in the upper and lower tercile.

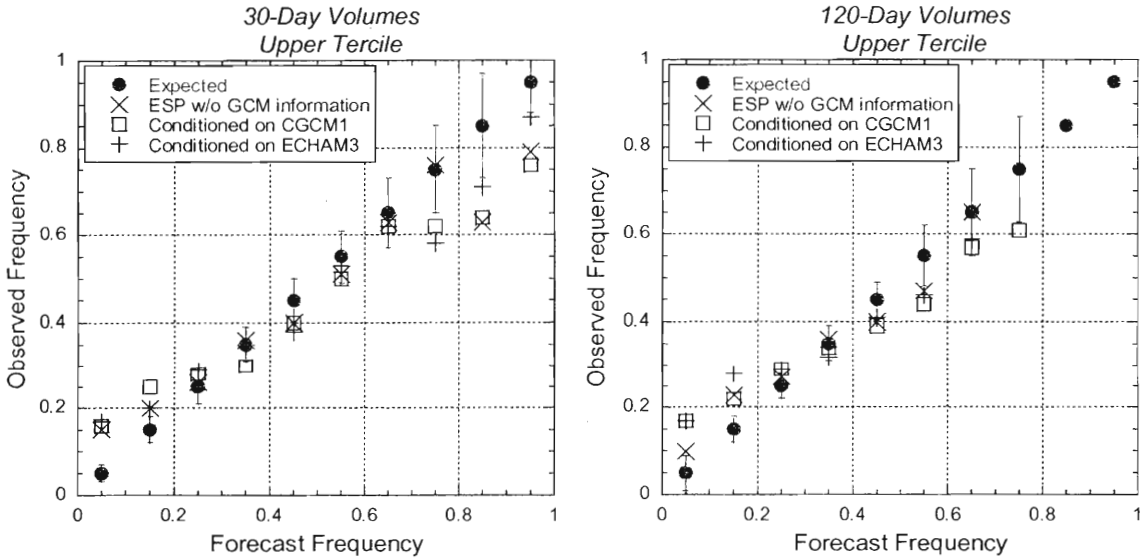

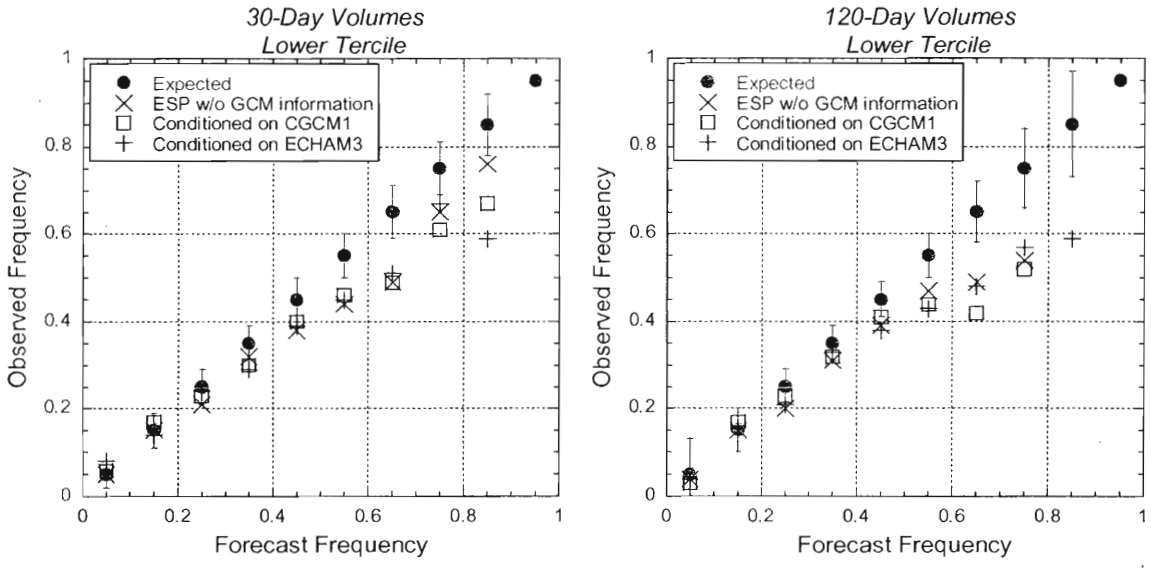

Figure 13. As in Figure 12 for Lake Norris.

The reliability of the forecasts over the entire range of forecast frequencies is summarized in the Brier score. The Brier scores for the 30-, 60-, 90-, and 120-day inflow volumes are presented graphically in Figure 14. The panels on the left side show the scores for Lake Lanier for volumes in the upper (upper panel) and lower (lower panel) terciles of the observed distributions, and likewise for the scores for Lake Norris on the right side. In all cases, except the 30-day Lake Lanier inflow volumes in the upper tercile, the Brier score is less than 0.1.

The plots for Lake Lanier show a decreaseing trend in Brier score as the inflow volume duration increases, although for the 120-day volumes in the lower tercile, there is a leveling-off or increase from the 90-day volumes. This supports the impression from Figure 13 that the reliability of forecasting volumes in the extreme terciles increases with the duration of the forecast.

In contrast to Lake Lanier, no distinct pattern in the Brier scores is identified for Lake Norris inflow volumes. The scores for volumes in the lower tercile are quite similar regardless of the duration of the forecast or the GCM-conditioning applied. For volumes in the upper tercile, the Brier score are smaller for the baseline ESP case than for either case of GCM-conditioning.

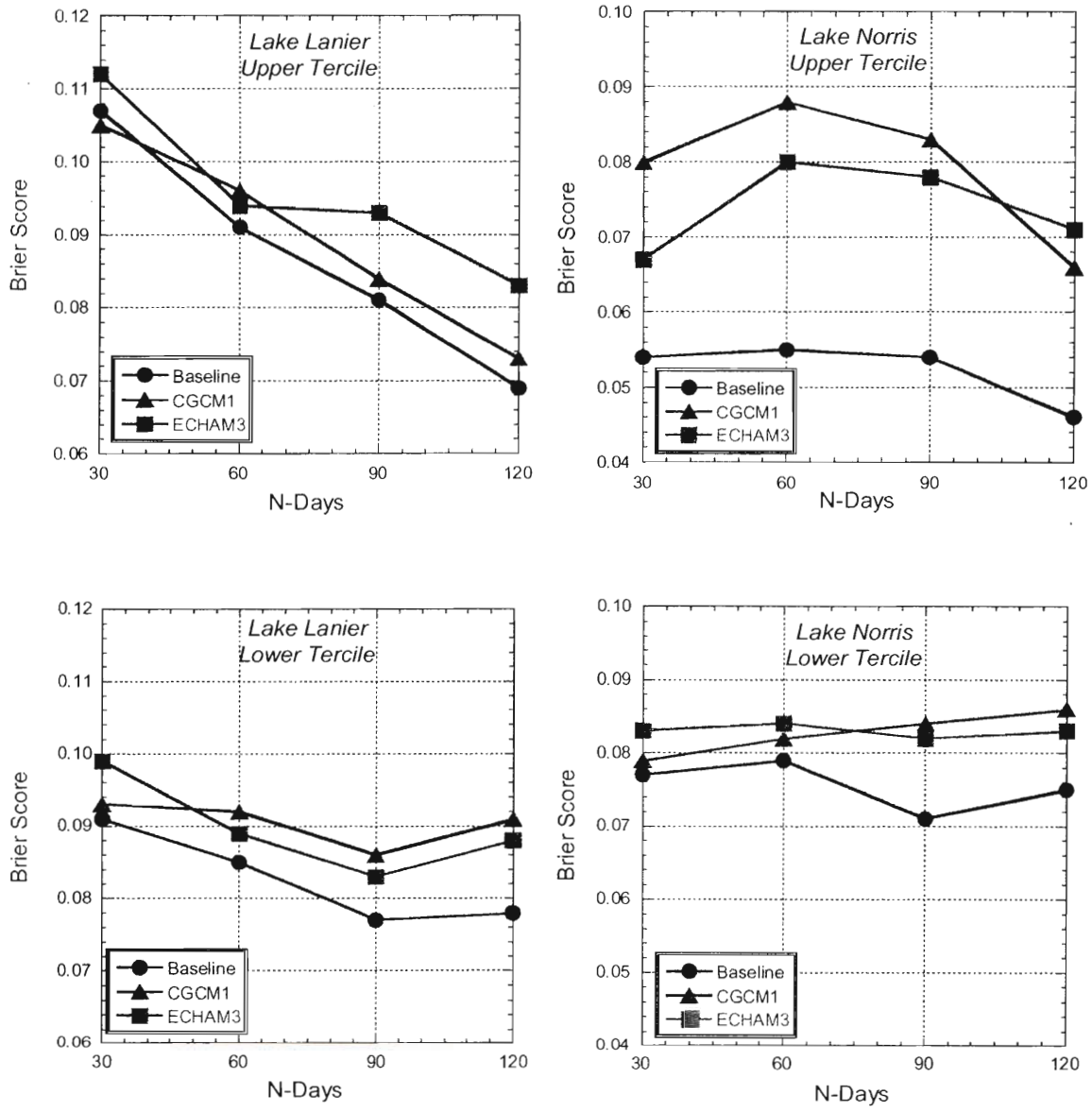

Figure 14. Brier score plotted as a function of the duration of inflow volume forecasts for Lake Lanier (left panels) and Lake Norris (right panels).

6. Reservoir Data

The decision support system is applied to two reservoirs Lanier and Norris. The main objectives for the management of both reservoirs are water supply, energy generation, and flood protection. Some system data are reported in this chapter. The conservation storages, elevation ranges, and power capacities are listed in Table 6.1.

Table 6.1: Reservoir Elevation Ranges

Reservoirs	Min Level (ft)	Max Level (ft)	Active Storage (bcf)	Power Capacity (MW)
Lanier	1035	1072	49.05	1X5+2X50=105
Norris	960	1034	83.7	2X73=146

Other reservoir data, including elevation versus storage curves, tail water curves, and hydro turbine characteristics are included in Appendix A.

The historical records used in this study are from 1950 to 1993 for Lanier, and 1959 to 1990 for Norris. The respective weekly average sequences are shown in Figures 15 and 16.

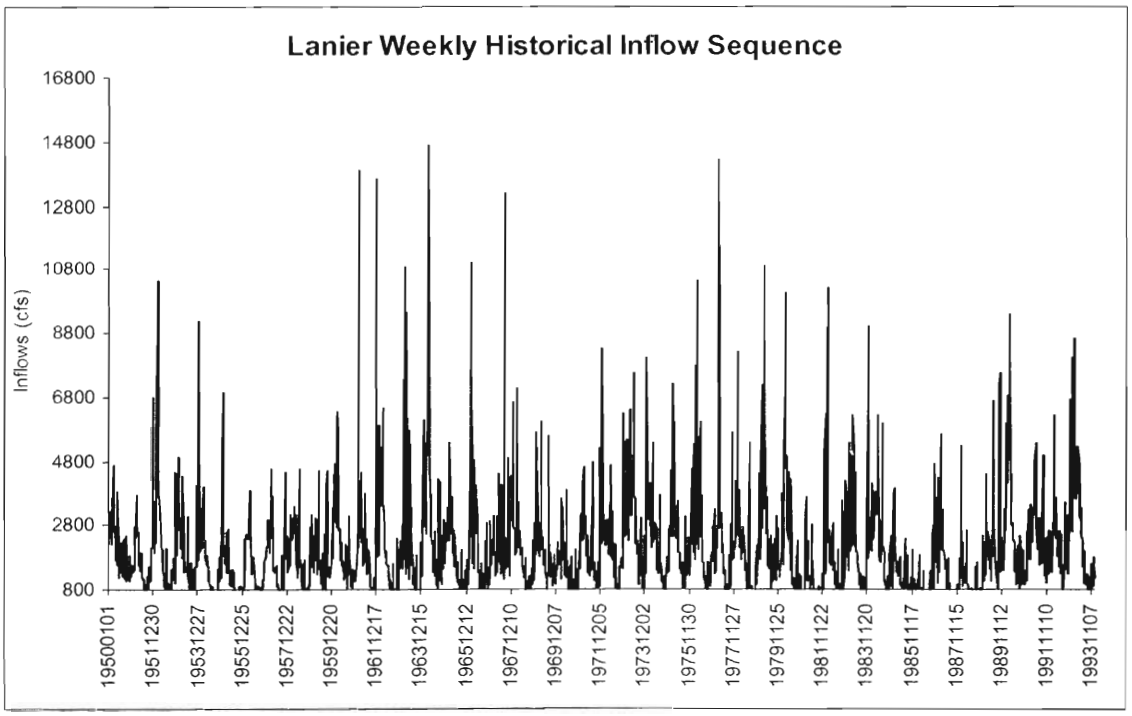

Figure 15: Historical Inflow Sequence for Lanier

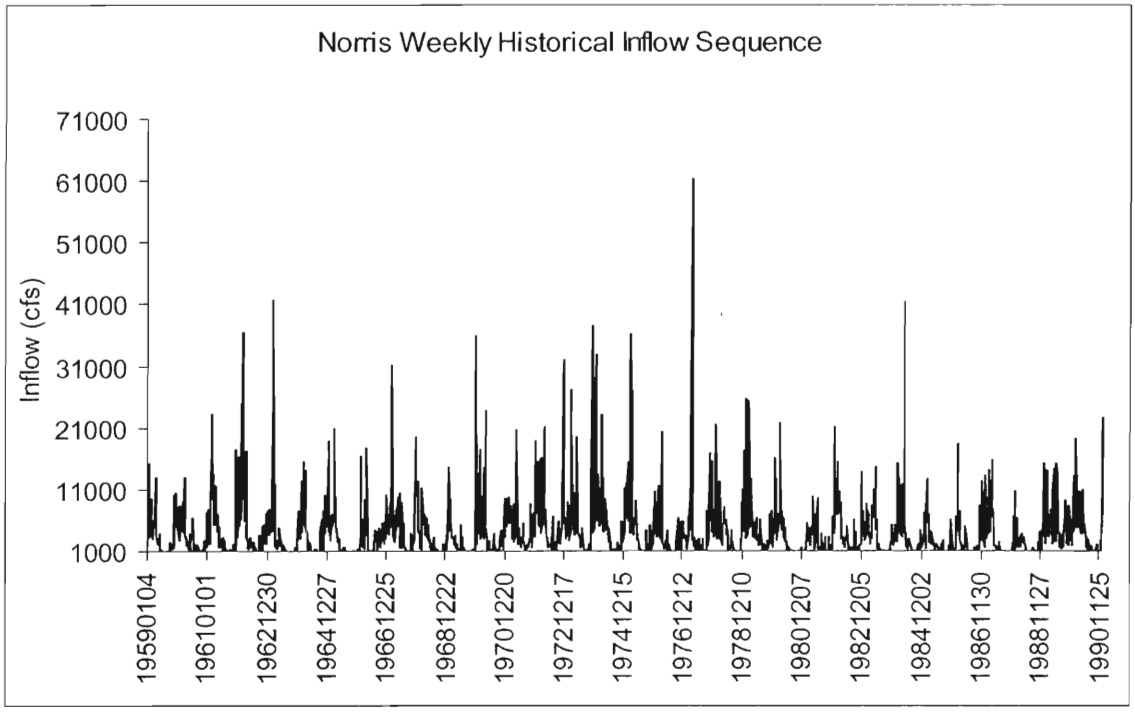

Figure 16: Historical Inflow Sequence for Norris

7. Control Models in the Decision Support System

The purpose of the control model in the decision support system is to identify tradeoffs among water availability, energy generation, and other water uses, and to develop a tentative plan for reservoir releases over a period of several months to a year using the forecasts presented in the previous chapters. The plan is meant to be reevaluated as time progresses and as more accurate information is collected on the state of the system, the hydrology, and the demands. Thus, the control model is designed to operate in a sequential and adaptive manner. The model has a weekly time resolution and a control horizon provided by the forecasting model. This chapter presents the control model formulation and solution methodology.

7.1. Reservoir Dynamics

The system response can be represented by the water balance relationship:

$$S(k+1) = S(k) + W(k) - R(k) - EVP(S(k)) - D(k)$$

k = 0, 1, 2, …, N-1.

In the above equation, k is the discretization time interval corresponding to one week; S(k) is reservoir storage at the beginning of the week; EVP(S(k)) is the net evaporation loss, which is a function of reservoir surface area and therefore storage; R(k) is the release volume during period k; W(k) is the local inflow volume; D(k) is water withdrawal from the reservoir, if any; and N is the control horizon in weeks.

Storage and release variables are constrained to be within certain feasible ranges as follows:

$$S^{min}(k) \le S(k) \le S^{max}(k), \; k = 1, 2, \ldots, N,$$

$$R^{min}(k) \le R(k) \le R^{max}(k), \; k = 0, 1, \ldots, N-1.$$

The upper and lower storage limits correspond to the reservoir conservation storage zones reported in the previous chapter. (Flood storage is not included in the conservation storage zone because the time resolution of the planning model is one week. Namely, this storage is always assumed available to accommodate high frequency hydrologic events.) The lower release limits are constrained by environmental and water supply requirements both of which can change seasonally. The upper release bounds are determined based on hydro turbine capacity and spillway capacity.

In view of the inflow uncertainty, the storage constraints are more properly expressed in a probabilistic form:

$$Prob[\, S_i^{min}(k) \le S\ (k)\,] \ge \pi^{min}(k)$$

$$Prob[\, S\ (k) \le S^{max}(k)\,] \ge \pi^{max}(k)$$

$$k = 0, 1, \ldots, N,$$

where π^{min} and π^{max} are reliability levels. These levels as well as the upper and lower storage and release thresholds are denoted here as time-varying but are usually time-invariant.

The goal of the control algorithm is to identify the release sequences $\{U^*(k), k=0,1, ..., N-1\}$ such that system objectives and constraints are met successfully. The element of the formulation that brings this to bear and also measures the success of the various operational alternatives is the performance index discussed next.

7.2. Performance Index

The purpose of the control model is to maximize the energy generation while meeting the various water supply and environmental requirements. To this end, the following performance index is adopted:

$$J = E\ \{ \sum_{k=0}^{N-1} [\ P_h(S(k)) + P_{strg}(S(k)) + P_{utrg}(U(k)) + P_{spl}(U(k)) + P_{en}(U(k), S(k))\ ] + P_h(S(N)) + P_{strg}(S(N))\},$$

where

$$P_h(S(k)) = a \left[\frac{[\ H^{\max} - H\ (S_i^{\pi^{\max}}(k))\ ]^2}{1 + e^{\frac{H^{\max} - H\ (S_i^{\pi^{\max}}(k))}{T_H}}} + \frac{[\ H\ (S_i^{\pi^{\min}}(k)) - H^{\min}\ ]^2}{1 + e^{\frac{H\ (S_i^{\pi^{\min}}(k)) - H^{\min}}{T_H}}} \right] ,$$

$$P_{strg}(S(k)) = \beta \left[\frac{[\ S\ (k) - S^{trg}(k)\ ]^2}{[S^{\max}(k) - S^{\min}(k)]^2} \right] ,$$

$$P_{utrg}(S(k)) = \gamma \left[\frac{[U\ (k) - U^{trg}(k)]^2}{[U^{\max}(k) - U^{\min}(k)]^2} \right] ,$$

$$P_{spl}(U(k)) = \delta\ SPL\ (U\ (k)) \quad ,$$

$$P_{en}(U(k), S(K)) = \varepsilon f(E(k)) \quad .$$

In the first above equation, E{ } denotes expectation of the quantity in the brackets with respect to the joint probability distribution of the reservoir inflows. There are five terms in the performance index.

The first term is intended to keep reservoir elevations within their respective bounds, $[H^{min}, H^{max}]$. Essentially, if the reservoir level is outside its bounds, P_h imposes a quadratic penalty.

The second term $P_{strg}(S(k))$ penalizes deviations away from some target state values. For the reservoir state variables, the target storage values are the storages that correspond to the upper limits of the conservation zones. Thus, the rationale of this term is to maintain high reservoir levels to conserve water and at the same time maximize turbine generation efficiency.

Similarly, the third term $P_{utrg}(U(k))$ penalizes deviations of the release variables away from certain desirable target values. Including this quadratic term also helps to improve the convergence rate of the optimization algorithm.

The fourth term, $P_{spl}(U(k))$, is a penalty for spillage. Spillage is the portion of release in excess of hydro turbine capacity. If possible, spillage should be avoided, because it bypasses the turbines and does not generate energy.

The fifth term, $P_{en}(U(k), S(k))$, is to maximize the energy generation. The penalty coefficient has a negative sign for the minimization problem.

Penalty coefficients α, β, γ, δ, and ε are used to introduce priorities in the performance index terms. In this model, these coefficients are determined such that the first term (level constraints) is dominant, followed by the fourth (spillage) and fifth (hydro energy) terms. The second and third terms are only introduced to convexify the optimization problem. These coefficients are calibrated through extensive sensitivity analysis.

7.3. Control Method

The control problem formulated in the previous section is solved using the Extended Linear Quadratic Gaussian (ELQG) control method, which was originally introduced by *Georgakakos and Marks, 1987,* and further developed by *Georgakakos 1989, 1991, 1993, Georgakakos et al., 1995a, Georgakakos and Yao, 1995,* and *Georgakakos et al., 1997a,b,c.* ELQG is an iterative optimization procedure starting from an initial control sequence $\{\mathbf{u}(k); k = 0, 1, 2, .., N-1\}$ and subsequently generating increasingly better sequences until convergence. Convergence is achieved when the value of the performance index cannot be reduced any further. ELQG is reliable, computationally efficient, and especially suited for uncertain, multi-reservoir systems. A more detailed account of the ELQG optimization algorithm and features are included in Appendix B and in the cited references.

7.4. Control-Simulation Process

To assess the system response under different forecasting scenarios, the above control model is applied sequentially to a selected historical inflow sequence. The assessment framework is shown on Figure 17. For each forecasting scenario, the assessment process is as follows: First, the forthcoming inflows are retrieved from the scenario selected. Next, the control model is activated to develop reservoir release and generation schedules. The release for the first week of the control horizon and the weekly inflows (unknown up to this time) are applied, and the system response (lake levels, releases, generation, spillage, water supply deficits, energy generation shortages, and energy generation value) is simulated and recorded. This process is repeated for the next week until the end of the assessment horizon. At the completion of the assessment process, the results are analyzed to provide quantitative measures of system response and to compare different scenarios. In what follows, we discuss several assessment applications for both Lanier and Norris.

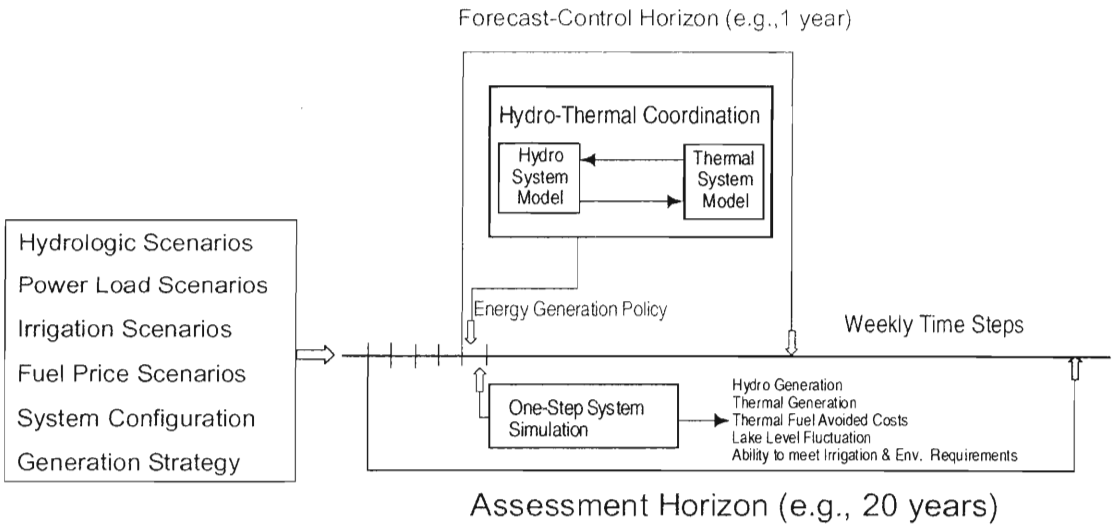

Figure 17: Scenario Assessment Framework

8. Applications of Decision Support System to Lanier and Norris Reservoirs

8.1. Simulation Results for Lanier

The control-simulation model is applied to Lanier using the historical inflow record from 1950 to 1993. The control targets are to (1) meet the projected water supply withdrawals for the year 2030, (2) meet instream flow requirements (pollution abatement); provide 2-hrs peak power generation per week day, (3) maintain high lake levels (hydropower/drought mgt), and (4) avoid spillage at 95% reliability. The projected demands for year 2030 are shown in Figure 18. The instream flow constraint requires Lanier, along with the contribution of the downstream tributary Peachtree Creek, to provide a minimum of 750 cfs river flow.

Figure 19 shows the comparison of the simulated elevation sequences under the baseline forecasting scheme and the CGCM-conditioned scheme. The results indicate that the system experienced a long drought period during which the projected 2030 demands could not be met. Figure 20 shows the corresponding release sequences. The results indicate that the lake sequences and performance are not significantly different between the baseline and the CGCM-conditioned forecasts. The lake levels are lower for CGCM-conditioned forecasts, and the CGCM forecasts cause higher high-end releases and lower low-end releases as shown on the lake release frequency plots in Figures 21 and 22. The CGCM-conditioned forecasts lead to more instream flow violations. Finally, the energy generation (peak generation/reliability and total generation) is somewhat less for CGCM-conditioned forecasts. The annual statistics are summarized in Table 8.1.

Table 7.1. Annual Simulated Statistics for Lanier

	Energy (GWH)	Min.Flow Voilation (%)
Baseline	159.89	0.56
CGCM	159.13	0.63

The overall benefit of baseline and CGCM-conditioned forecasts is low. This is due to (**1**) the large lake storage and turbine outflow capacity in relation to inflows; and (**2**) the management decisions are mainly driven by demands and reservoir levels. Baseline forecasts perform somewhat better due to their narrower ensemble range.

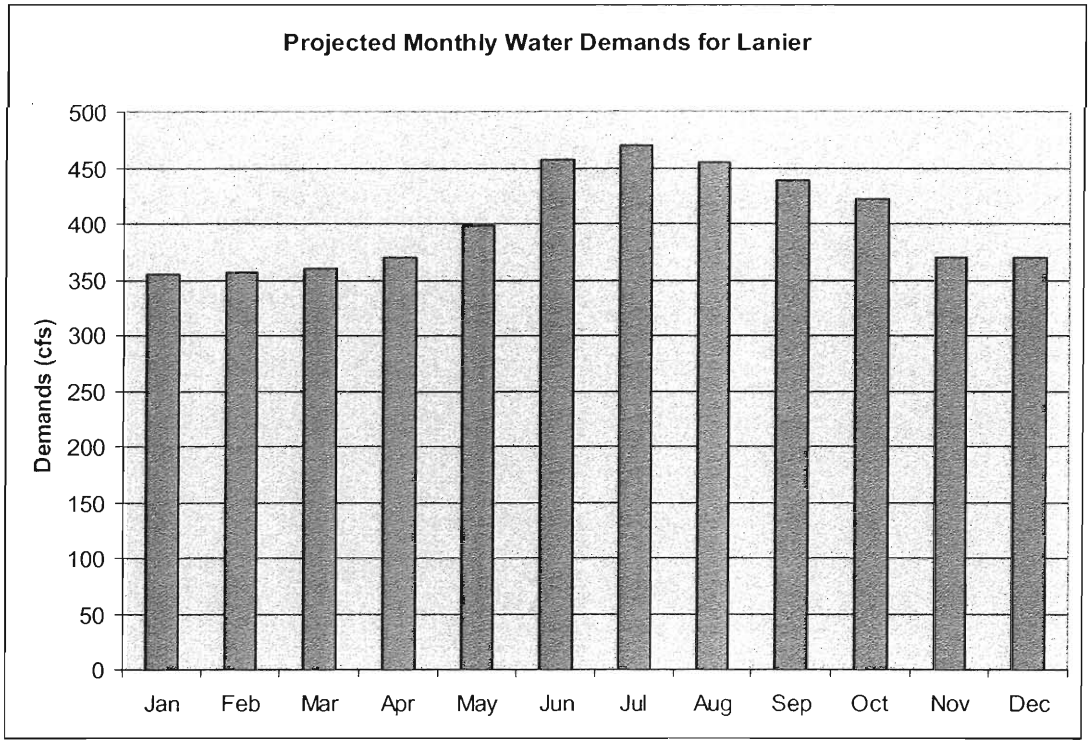

Figure 18: Projected 2030 Demands for Lanier

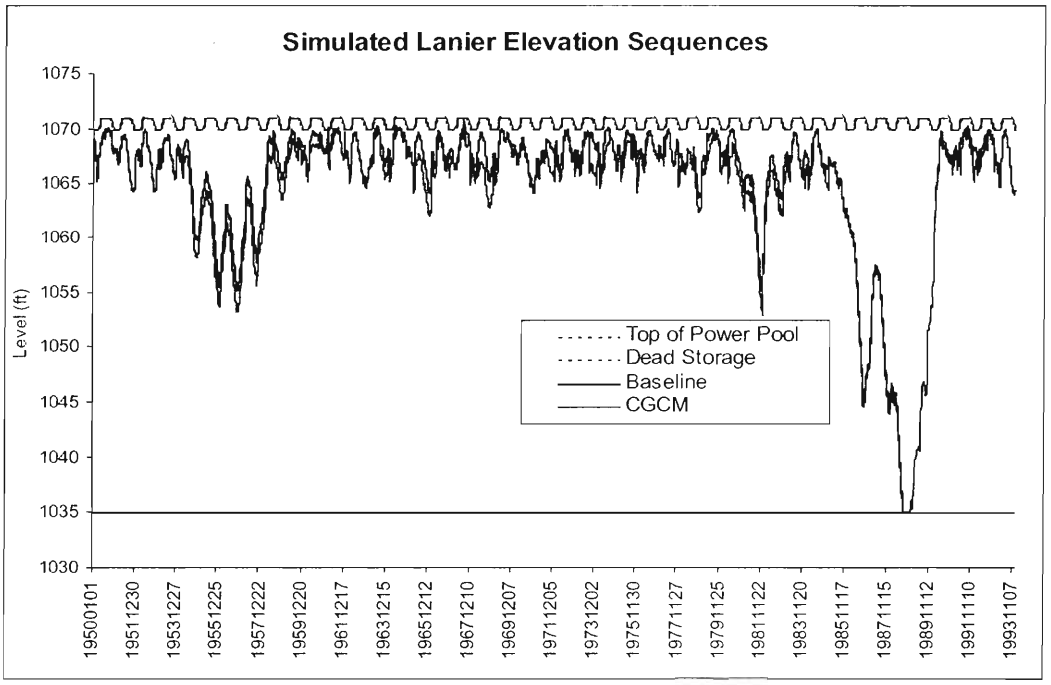

Figure 19: Simulated Lanier Elevation Sequences

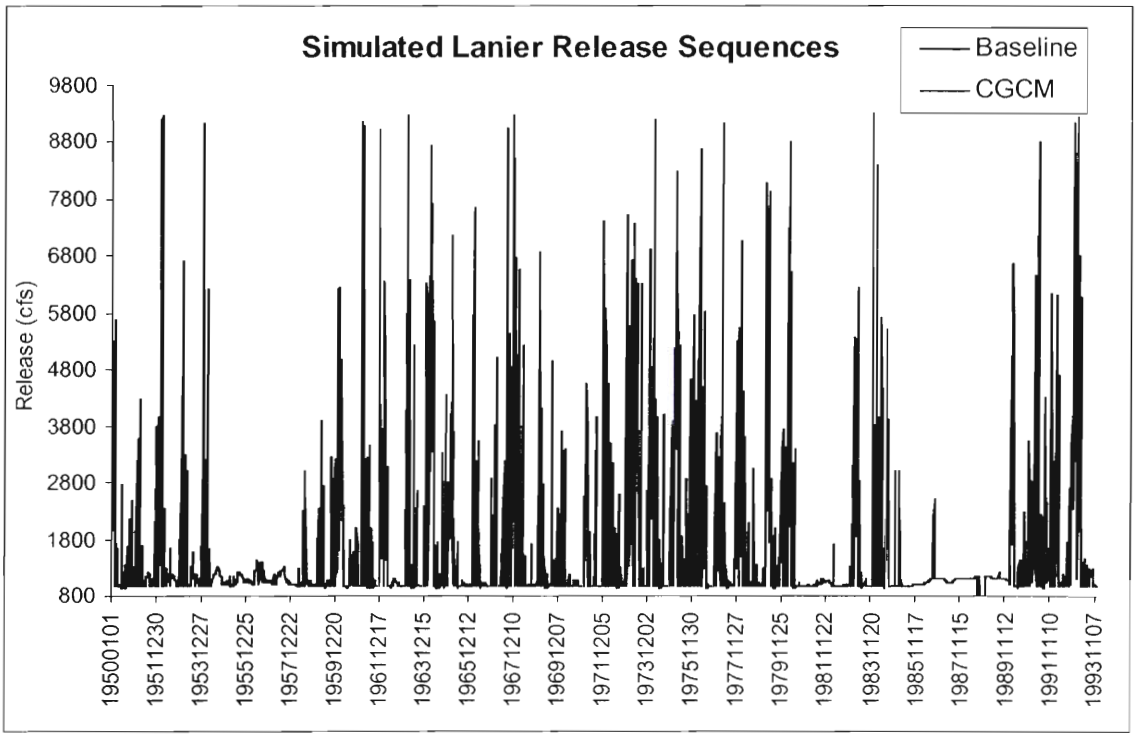

Figure 20: Simulated Lanier Release Sequences

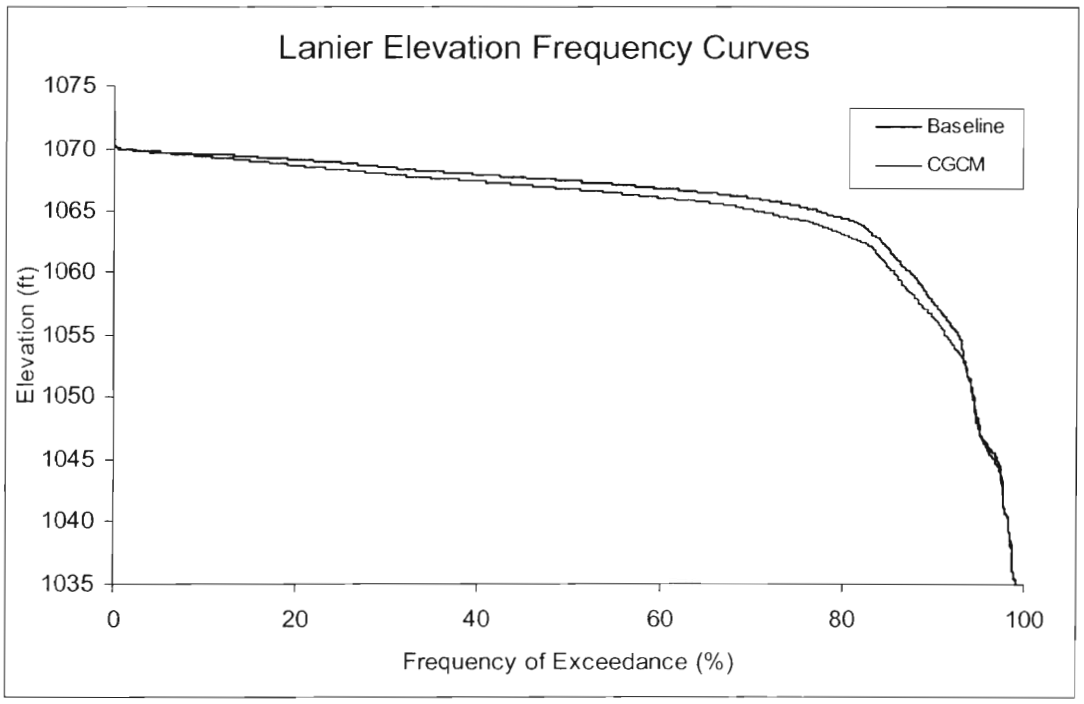

Figure 21: Simulated Lanier Release Sequences

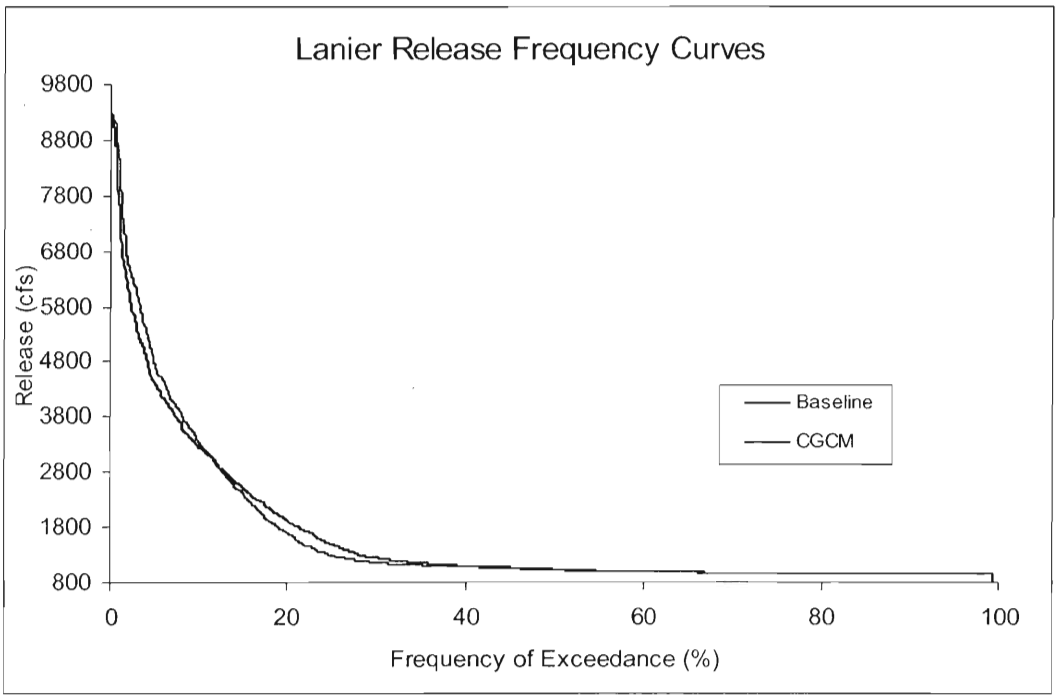

Figure 22: Simulated Lanier Release Sequences

8.2. Simulation Results for Norris

The control-simulation model is applied to Norris using the historical inflow record from 1959 to 1990. The control targets are to maintain high lake levels for hydropower and drought management, generate as much energy as possible, and avoid spillage at 95% or higher reliability. Four different forecasting schemes are examined: Baseline, CGCM, ECHAM, and Perfect. The Perfect forecast scenario assumes perfect knowledge of upcoming inflows in the control model. It is the upper bound of all forecasts and provides a good base for assessing the benefit of improvement from the forecasting techniques.

Figures 23 to 26 show the simulated elevation, release, and energy sequences for all forecasting schemes. Lake sequences and performance are not significantly different for baseline, CGCM, and ECHAM forecasts. However, ECHAM performs somewhat better than both baseline and CGCM with respect to energy generation, annual spillage, and maximum outflow. In particular, ECHAM reduces maximum outflow by about 12%. The annual statistics are summarized in Table 8.2. Perfect forecasts would potentially lead to significant improvements, exhibiting higher reservoir levels 95% of the time, 35% lower maximum release for flood protection, higher and more reliable low flows for drought management, and 8% more energy generation. The comparison plots of frequency curves are shown in Figures 27 to 29.

Table 8.2: Annual Statistics for Norris

	Energy (GWH)	Annual Spillage (bcf)	Max. Release (cfs)
Baseline	439.65	9.79	48986.76
CGCM	439.67	9.39	48818.88
ECHAM	440.03	9.34	42685.22
Perfect	475.34	0.89	31532.59

The overall benefit of baseline and CGCM forecasts is low, while ECHAM demonstrates some skill in forecasting high precipitation events (exhibiting more reliable forecast ensembles) and improves flood management. The performance sensitivity to forecasting is diminished because of the dynamic operational rules generated by the decision system. The perfect forecast

sequences, though an ideal scenario, indicate that lake management would benefit from increased forecast skill both in short term and long term.

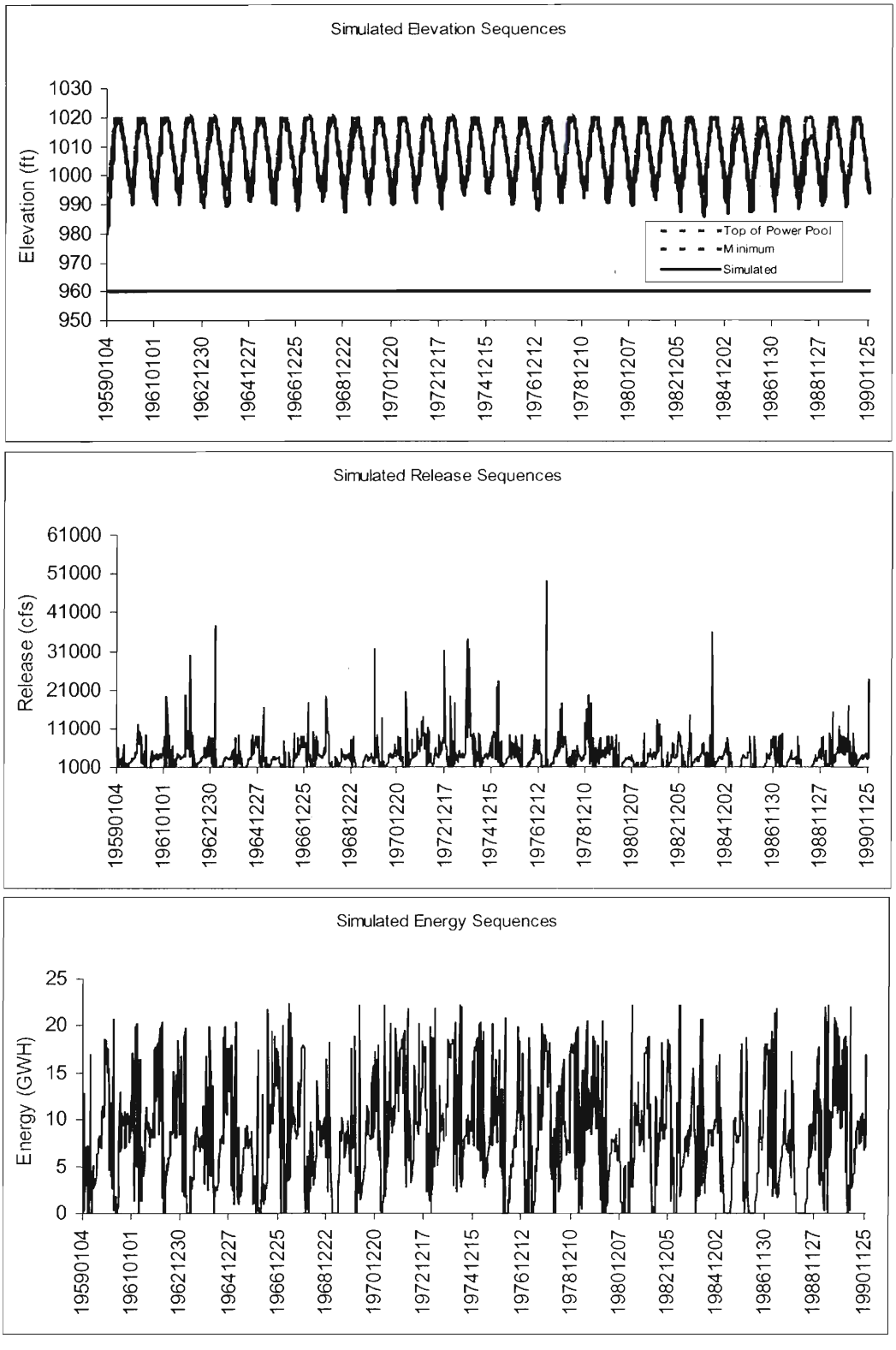

Figure 23: Simulated Sequences for Norris; Baseline Forecasts

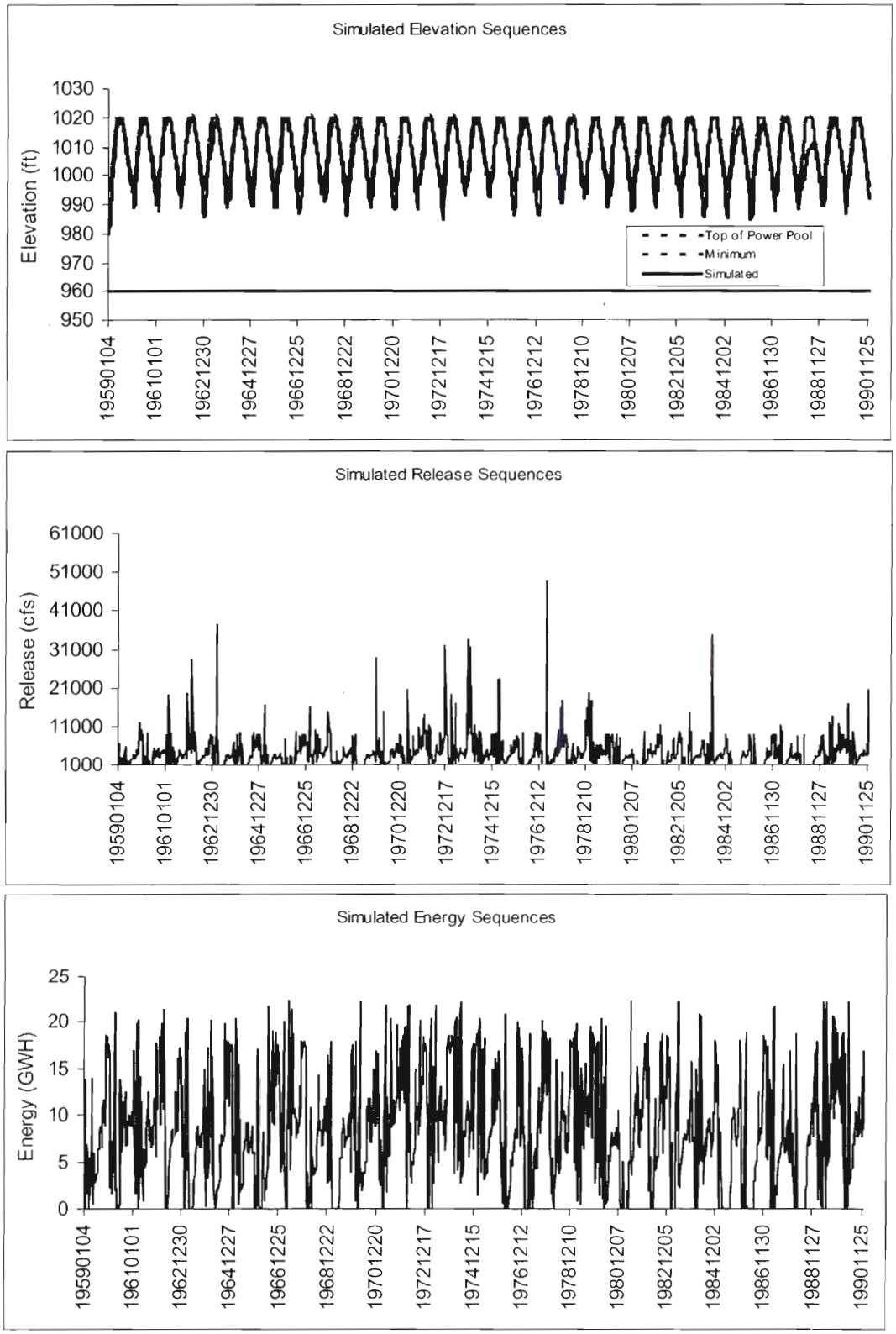

Figure 24: Simulated Sequences for Norris; CGCM Forecasts

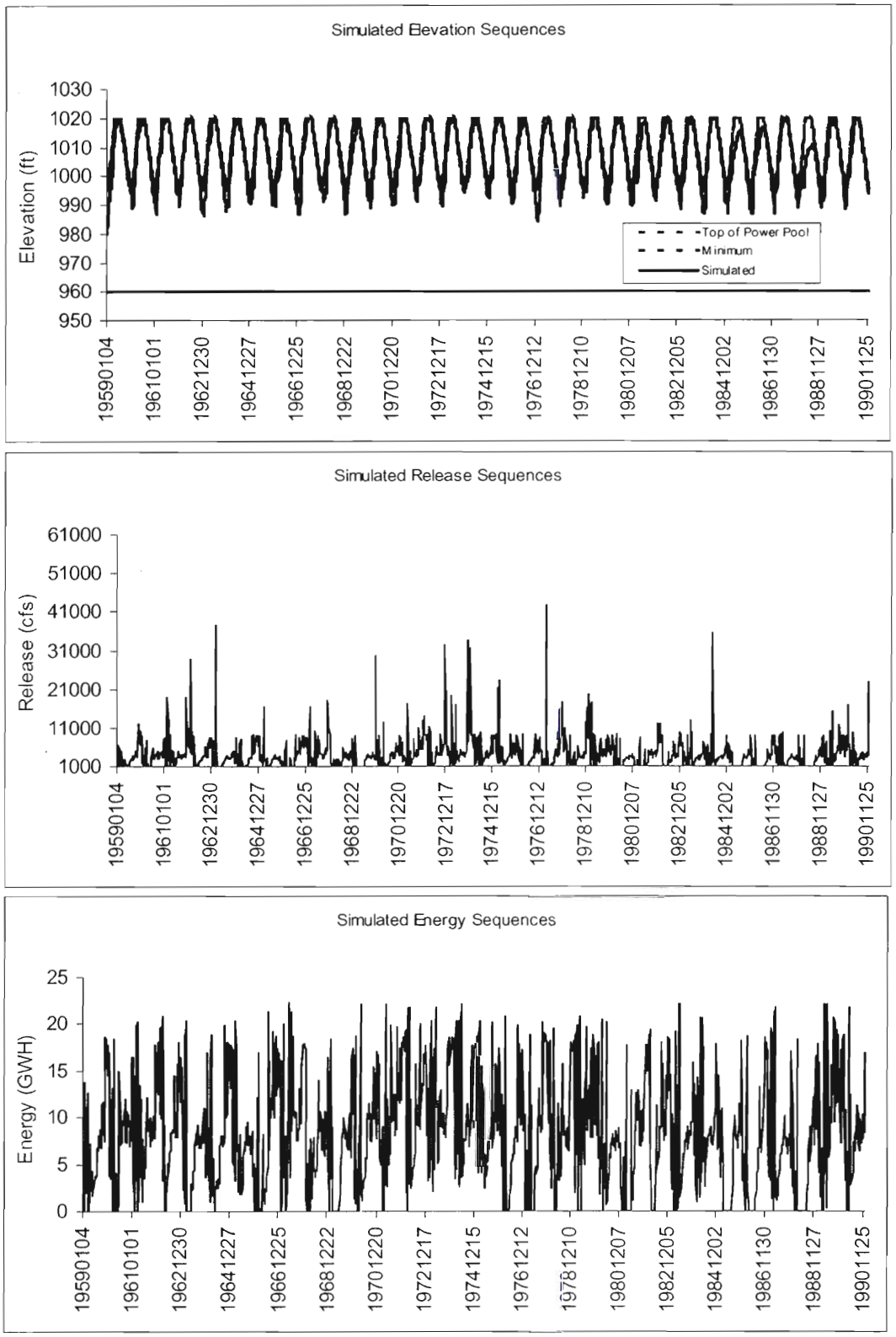

Figure 25: Simulated Sequences for Norris; ECHAM Forecasts

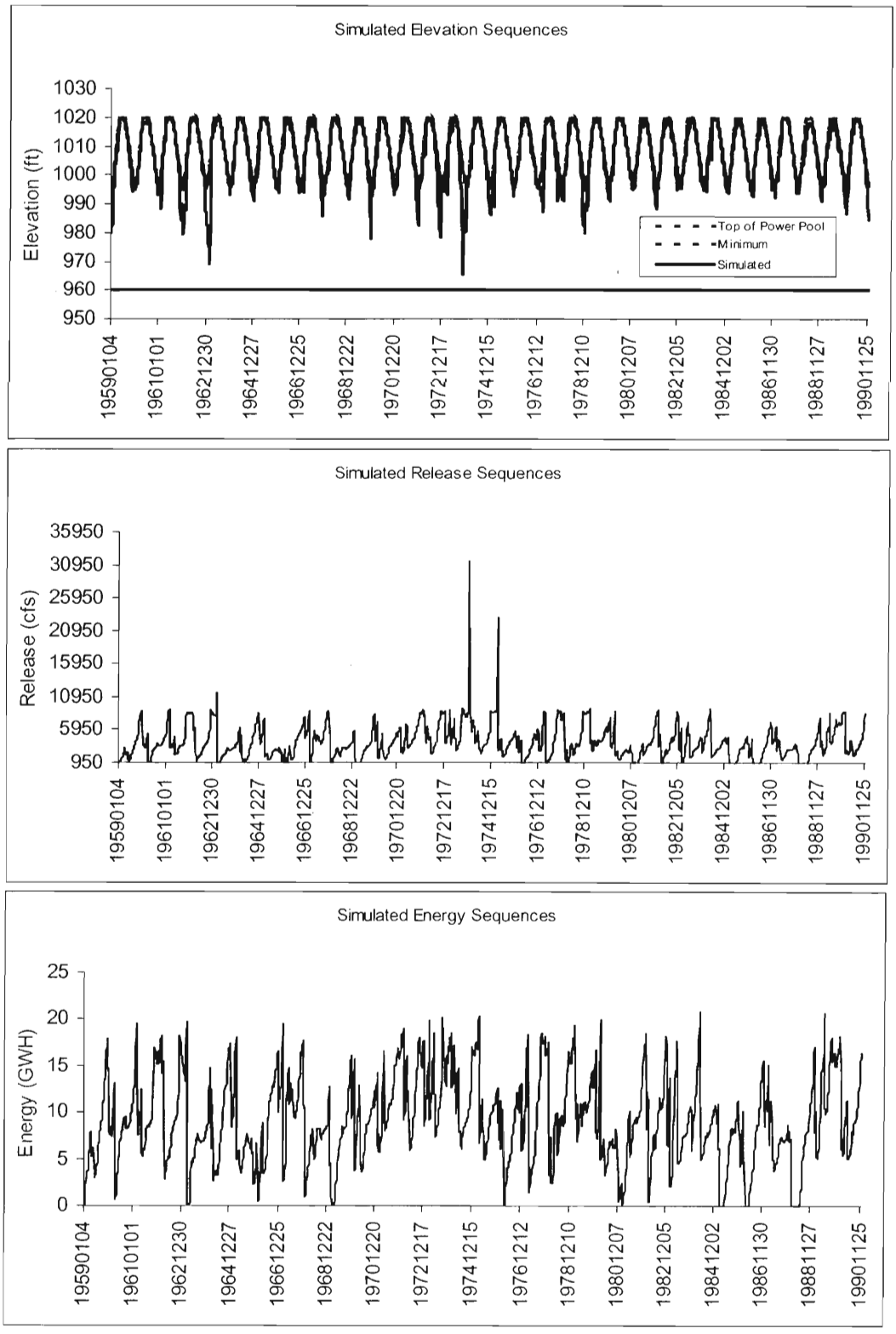

Figure 26: Simulated Sequences for Norris; Perfect Forecasts

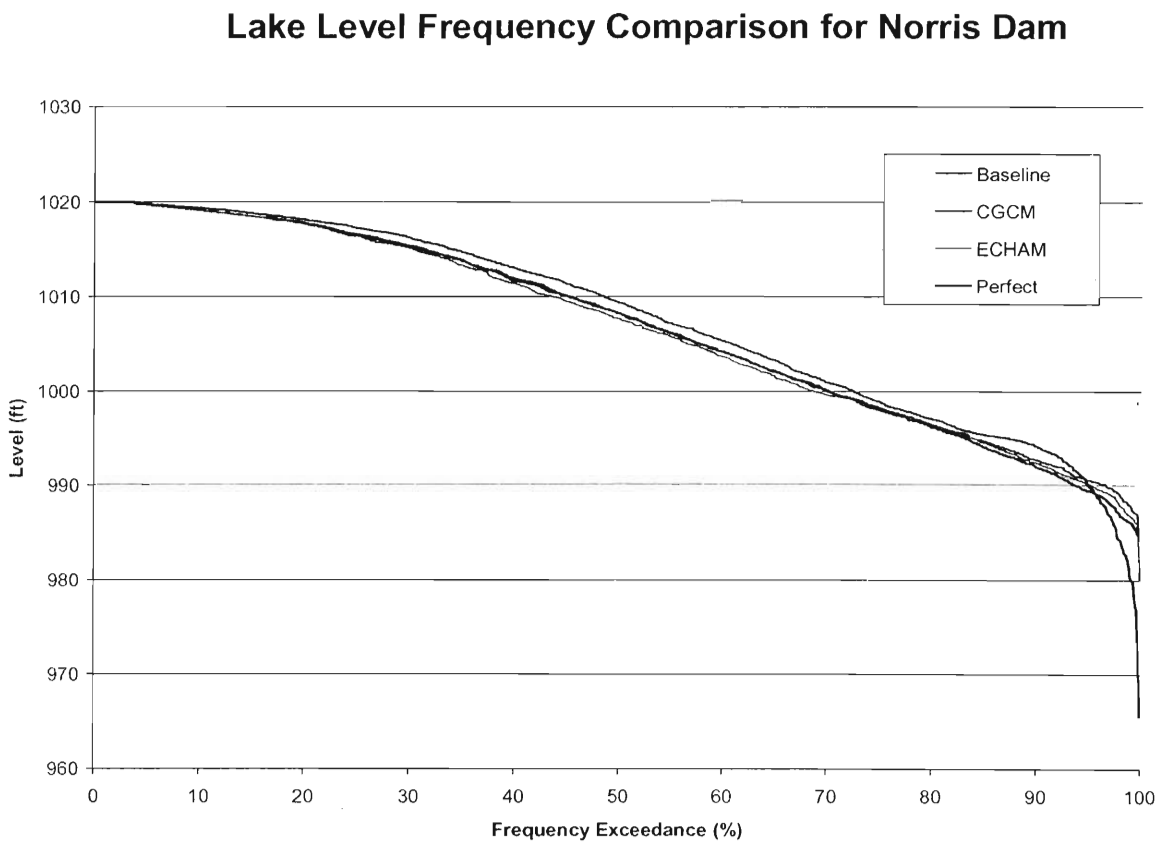

Figure 27: Simulated Elevation Frequency Curves for Norris

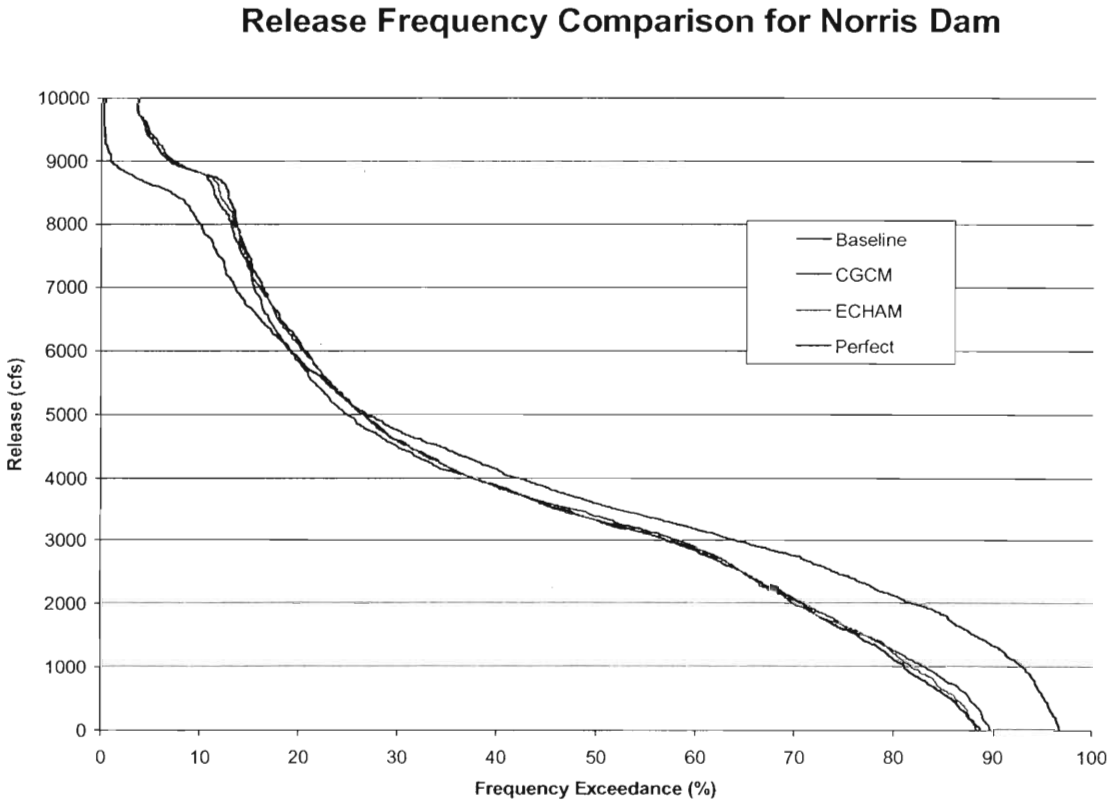

Figure 28: Simulated Release Frequency Curves for Norris

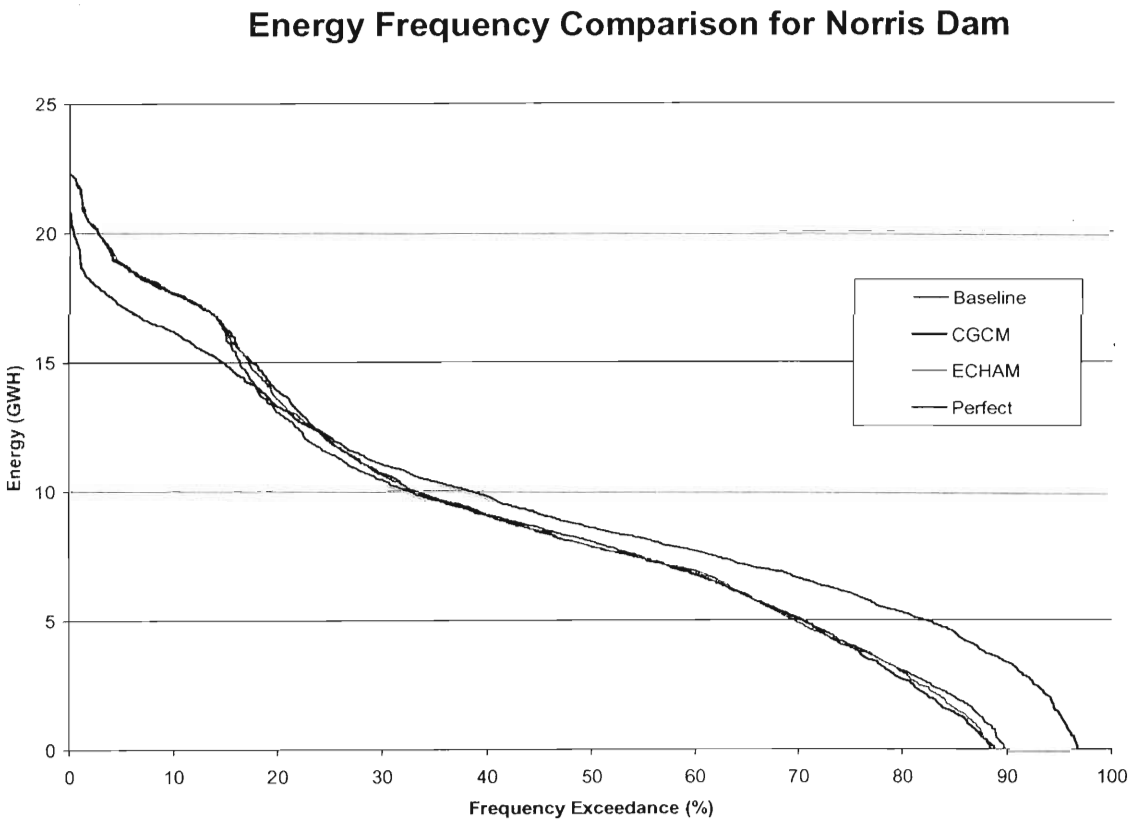

Figure 29: Simulated Energy Frequency Curves for Norris

9. Conclusions (need paragraph for decision system)

This report presents the methodology of an integrated forecast-control system for reservoir hydrosystems, which incorporates climate information from Global Climate Models (Figure 1), and its applications to two watersheds in the Southeastern United States. The use of the system in terms of ensemble reservoir inflow forecasts is demonstrated, where the forecast component is applied with and without GCM information. For the system applied with GCM information, both an atmospheric (the ECHAM3 model) and a coupled ocean-atmosphere (the CGCM1 model) GCMs are used.

The first step in linking the GCM information to the integrated model components is to downscale the GCM forecasts. This is necessary to extract from the GCM, which has a scale of approximately 100,000 km^2, information that can be used advantageously at the scale of the watershed, a few thousand square kilometers. For the study watersheds, little correlation was obtained between the basin-averaged monthly precipitation and the nodal precipitation values for the two GCM datasets. This lack of correlation appears to be a factor when downscaling the GCM information to the input of the hydrologic model and the downscaling is based on terciles of the GCM distribution. Little difference was shown between the cumulative distributions of daily basin precipitation for periods when the GCM is in the upper tercile of its distribution and for periods when the GCM is in the lower tercile. This is found for both the CGCM1 and ECHAM3 datasets with respect to both study basins.

Reliability diagrams show that for both reservoirs the ensemble inflow forecasts produce reliable forecasts of inflow volumes in the extreme terciles of the observed volume distributions for forecast frequencies to approximately 0.6. This was found for various volume durations up to 120 days. For Lake Lanier inflow volumes, there appears to be an increase in the reliability of forecasting in the extreme tercile with longer volume duration.

(Please add a paragraph for the decision support system.)

ACKNOWLEDGEMENTS:

This work was sponsored by the NOAA through NOAA Grant No. NA76GP0352 for Lake Lanier, and through NOAA Grant No. NA96GP0408, GIT Subcontract No. E-20-F21-G1 for Lake Norris. The authors thank Dr. Aris Georgakakos and Dr. Huaming Yao, of the Georgia Water Resources Institute, for their collaboration throughout these projects. We also gratefully acknowledge the comments and suggestions of Dr. Nick Graham, of HRC and Scripps Institution of Oceanography, on climate model issues and particularly the ECHAM3 model forecasts. Steve Taylor, of HRC and Scripps, also assisted with the model runs for Lake Norris. The efforts of Mr. James E. Hathorn, Jr., of the U.S. Army Corps of Engineers Mobile District, in supplying unimpaired flow data and documentation for Lake Lanier, and of Dr. Stuart Schwartz, formerly with HRC, toward the initial calibration of Lake Norris hydrologic model, are recognized.

REFERENCES:

Benjamin, J.R., and C.A. Cornell, 1970: *Probability, Statistics, and Decision for Civil Engineers*. McGraw-Hill Co., New York, 684pp.

Busuioc, A., von Storch, H., and R. Schnur, 1999: Verification of GCM-generated regional seasonal precipitation for current climate and of statistical downscaling estimates under changing climate conditions. *J. Climate*, **12**, 258-272.

Carpenter, T.M., and K.P. Georgakakos, 2001: Assessment of Folsom Lake response to historical and potential future climate scenarios: 1. Forecasting. *J. Hydrology*, **249**, 148-175.

Day, G.N., 1985: Extended streamflow forecasting using the NWSRFS. *J. Waters Resources Planning and Management*, **111**(2) 157-170.

Gates, W. L., 1992a: AMIP: The Atmospheric Model Intercomparison Project. *Bull. American Meteorological Society*, **73**(12), 1962-1970.

Gates, W.L., 1992b: The validation of atmospheric models. *PCMDI Report No. 1*, Program for Climate Model Diagnosis and Intercomparison, Lawrence Livermore National Laboratory, Livermore, California.

Georgakakos, K.P., Georgakakos, A.P., and N.E. Graham, 1998: Assessment of benefits of climate forecasts for reservoir management in the GCIP region. *GEWEX News*, **8**(3), 5-7.

Georgakakos, K.P., 1986: A generalized stochastic hydrometeorological model for flood and flash-flood forecasting, 1: Formulation and 2: Case Studies. *Water Resources Research*, **22**(13), 2085-2106.

Georgakakos, A., and D. Marks D (1987). A New Method for the Real-Time Operation of Reservoir System, *Water Resources Research,* **23 (7),** 1376-1390

Georgakakos, A., (1989a). Extended Linear Quadratic Gaussian Control for the Real-Time Operation of Reservoir Systems. Esogbue A. In the book entitled DYNAMIC PROGRAMMING

FOR OPTIMAL WATER RESOURCES SYSTEMS ANALYSIS. 329-360. Prentice Hall Publishing Company, New Jersey.

Georgakakos, A., (1989b). Extended Linear Quadratic Gaussian (ELQG) control: Further extensions, *Water Resources Research,* **25 (2),** 191-201.

Georgakakos, A., (1993). Operational tradeoffs in reservoir control. *Water Resources Research,* **29 (11),** 3801-3819

Georgakakos, A., and H. Yao (1995). A Decision Support System for the Equatorial Lakes. Technical Report No. GIT/CEE-HYDRO-95-7, School of Civil and Environmental Engineering, Georgia Tech, Atlanta.

Georgakakos, A., H. Yao, and Y. Yu (1997a). A Control Model for Dependable Hydropower Capacity Optimization. *Water Resources Research,* **33 (10),** 2349-2365.

Georgakakos, A., H. Yao, and Y. Yu (1997b). Control Models for Hydroelectric Energy Optimization. *Water Resources Research*, **33 (10),** 2367-2379.

Georgakakos, A., H. Yao, and Y. Yu (1997c). A Control Model for Hydroelectric Energy Value Optimization. *ASCE Journal for Water Resources Planning and Management,* **123 (1),** 30-38.

Hengeveld, H.G., 2000: Projections for Canada's climate Future: A discussion of recent simulations with the Canadian Global Climate Model. Climate Change Digest, 00-01, Minister of Public Works and Government Services, Ontario.

Meehl, G.A., Boer, G.J., Covey, C., Latif, M., and R.J. Stouffer, 1997: Intercomparison makes for a better climate model. *Eos*, **78**(41), 445-451.

Sailor, D.J., and X. Li, 1999: A semiempirical downscaling approach for prediction regional temperature impacts associated with climate change. *J Climate*, **12**, 103-114.

Yao, H., and A.P. Georgakakos, 2000: Assessment of Folsom Lake response to historical and potential future climate scenarios: 2. Reservoir Management. *J. Hydrology*, **249**, 176-196.

Appendix A: Reservoir Characteristic Curves

A.1. Elevation vs. Storage Curves

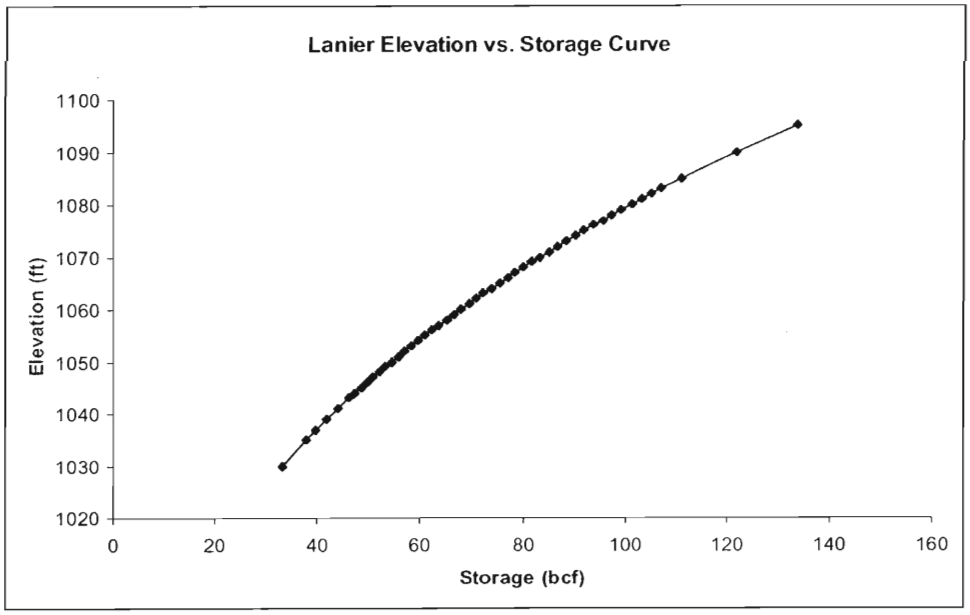

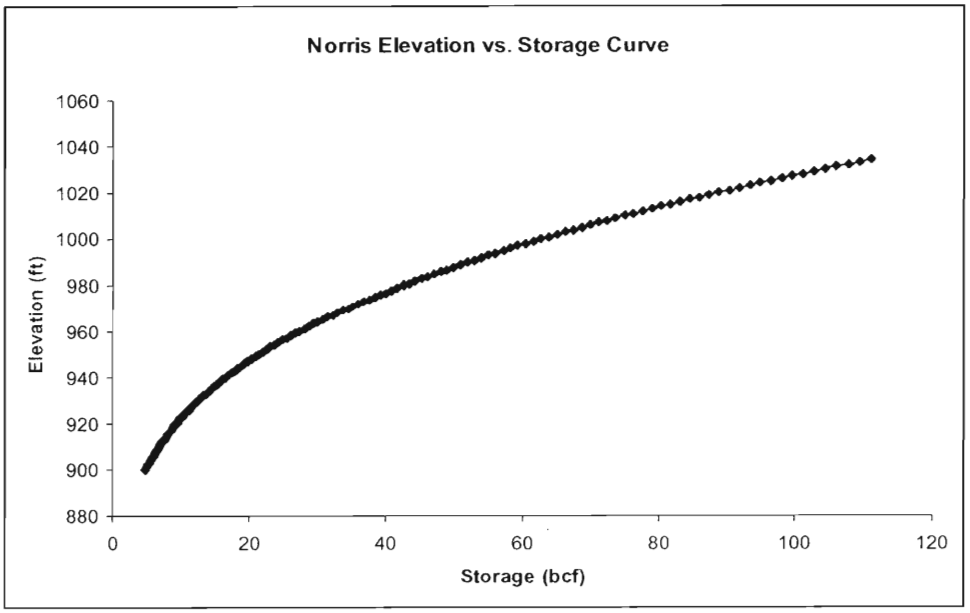

A.2. Tail Water Elevation vs. Discharge Curves

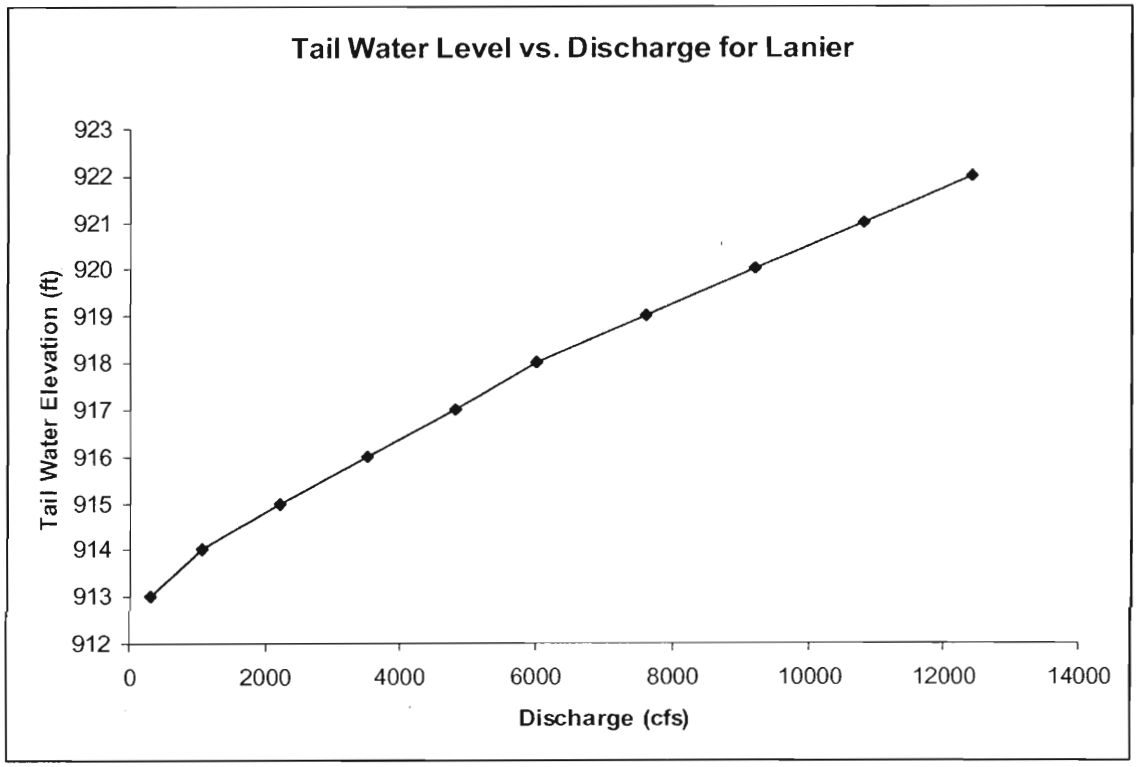

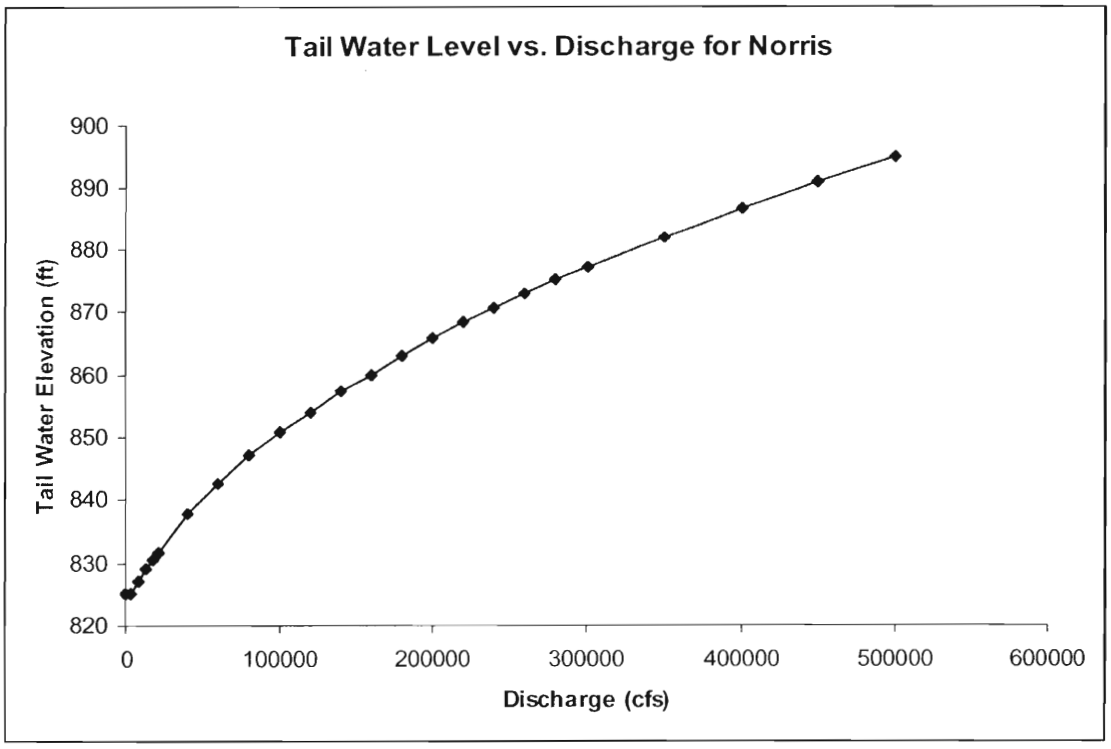

A.3. Turbine Characteristic Curves

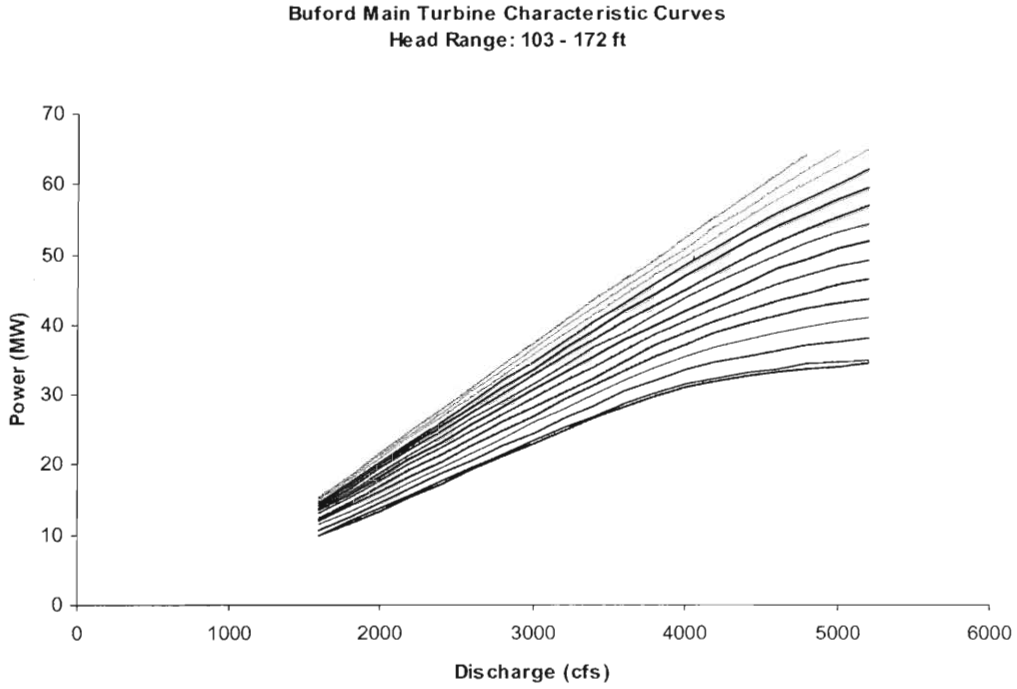

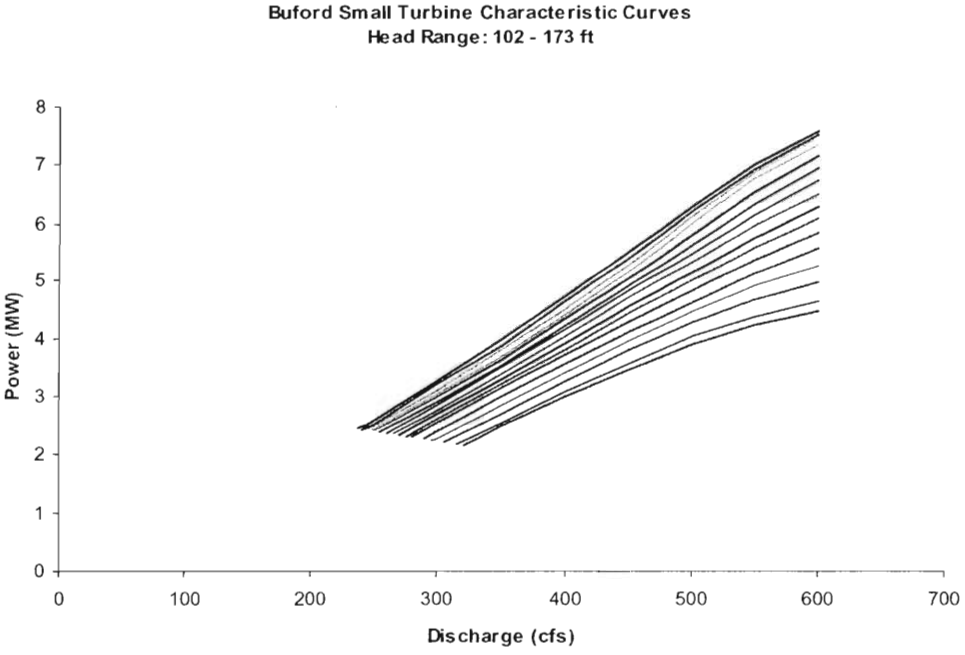

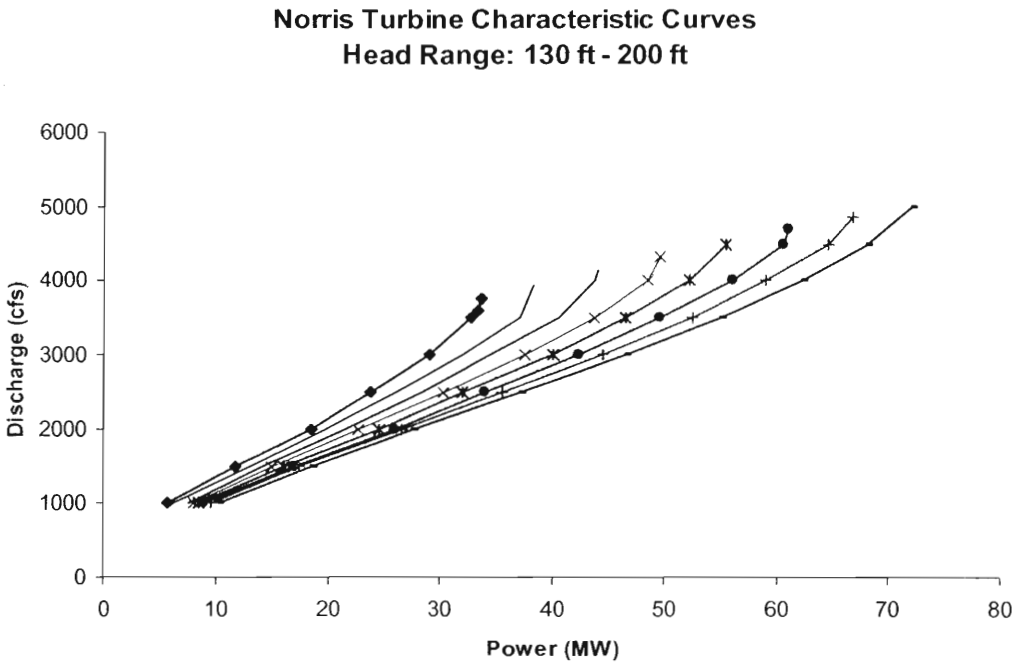
Norris Turbine Characteristic Curves
Head Range: 130 ft - 200 ft
Discharge (cfs)
6000
5000
4000
3000
2000
1000
0
0
10
20
30
40
50
60
70
80
Power (MW)

Appendix B. ELQG Control Method

The control problems formulated in this report are solved using the Extended Linear Quadratic Gaussian (ELQG) control method which was originally introduced by *Georgakakos and Marks, 1987,* and further developed by *Georgakakos 1989, 1991, 1993, Georgakakos et al., 1995a, Georgakakos and Yao, 1995,* and *Georgakakos et al., 1997a,b,c.* ELQG is an iterative optimization procedure starting from an initial control sequence $\{\mathbf{u}(k); k = 0, 1, 2, .., N-1\}$ and subsequently generating increasingly better sequences until convergence. Convergence is achieved when the value of the performance index cannot be reduced any further. ELQG is reliable, computationally efficient, and especially suited for uncertain, multi- reservoir systems. A short account of the ELQG optimization procedure and features follows next.

The optimal control problem includes three elements: system dynamics, constraints, and performance index. These can be expressed in the following general form:

$ System Dynamics:

$$S(k+1) = f\,[\,S(k)\,,\,u(k)\,,\,\xi(k)\,,\,k\,]$$

$$k = 0\,,1\,,\ldots,\,N-1 \quad ,$$

$ Constraints:

$$\text{Prob}[\,H_i^{min}(k) \le H_i(S_i(k))\,] \ge \pi_i^{min}(k)$$

$$\text{Prob}[\,H_i(S_i(k)) \le H_i^{max}(k)\,] \ge \pi_i^{max}(k)$$

$$u_i^{min}(k) \le u_i(k) \le u_i^{max}(k) \quad ,$$

$$i = 1\,,2\ldots,8, \;\; k = 0\,,1\,,\ldots,\,N\,,$$

These are associated with the system reservoirs and should be expressed in a probabilistic form due to the uncertain system nature.

$ Performance Index:

$$\underset{u(k),\ k=0,1,\ldots,N-1}{\text{Minimize}}\ J = E\left\{\ \sum_{k=0}^{N-1} g_k\,[\,S(k)\,,\,u(k)\,] + g_N[S(N)]\ \right\},$$

where **S**(k), **u**(k), and ξ(k) are the state, control, and uncertain input vectors, π_i^{min} and π_i^{max} are reliability parameters, g_k is a function including all performance index terms associated with period k, and g_N is a function including terms associated with the terminal time N. (As before, bold type indicates vector or matrix quantities.)

The Extended Linear Quadratic Gaussian (ELQG) solution procedure starts with an initial control sequence $\{ u^0(k) , \quad k = 0,1,...,N-1 \}$ and the corresponding mean state

$$\bar{S}^0(k+1) = f[\bar{S}^0(k), u^0(k), \bar{\xi}(k), k]$$

$$\bar{S}^0(0) = S(0) = \text{known} \quad ,$$

$$k = 0,1,...,N-1 \quad ,$$

sequence $\{\bar{S}^0(k) , \quad k = 0,1,...,N\}$:

where $\bar{\xi}(k)$ represents the mean of the random processes. The next step is to define a perturbation model valid around these nominal state and control sequences:

$$\Delta S(k) = S(k) - \bar{S}^0(k), \quad k = 0,1,...,N,$$

$$\Delta u(k) = u(k) - u^0(k), \quad k = 0,1,...,N-1,$$

$$\Delta \xi(k) = \xi(k) - \bar{\xi}(k), \quad k = 0,1,...,N-1,$$

This model describes the dynamic relationship of the state, control, and input vector perturbations, and has the following form:

$$\Delta S(k+1) = A(k)\ \Delta S(k) + B(k)\ \Delta u(k) + C(k)\ \Delta \xi(k) \ ,$$

$$\Delta S(0) = 0 \ ,$$

$$k = 0,1,..., N-1 \ ,$$

where the matrices **A**(k), **B**(k), and **C**(k) represent the gradient matrices of the state transition function with respect to the state, control, and input vectors respectively:

$$A(k) = \nabla_{S(k)}\ f(k) = \begin{bmatrix} \frac{df_1(k)}{dS(k)} \\ \frac{df_2(k)}{dS(k)} \\ M \\ \frac{df_n(k)}{dS(k)} \end{bmatrix}, B(k) = \nabla_{u(k)}\ f(k) = \begin{bmatrix} \frac{df_1(k)}{du(k)} \\ \frac{df_2(k)}{du(k)} \\ M \\ \frac{df_n(k)}{du(k)} \end{bmatrix}, C(k) = \nabla_{\xi(k)}\ f(k) = \begin{bmatrix} \frac{df_1(k)}{d\xi(k)} \\ \frac{df_2(k)}{d\xi(k)} \\ M \\ \frac{df_n(k)}{d\xi(k)} \end{bmatrix}.$$

The performance index is also expressed in terms of the perturbation variables as follows:

$$J = E\ \{\sum_{k=0}^{N1} [\frac{1}{2}\ \Delta S^T(k)\ Q_{SS}(k)\ \Delta S(k) + q_S{}^T(k)\ \Delta S(k)$$

$$+ \frac{1}{2}\ \Delta u^T(k)\ R_{uu}(k)\ \Delta u(k) + r_u{}^T(k)\ \Delta u(k) + \Delta u^T(k)\ Q_{uS}(k)\ \Delta S(k)]$$

$$+ \frac{1}{2}\ \Delta S^T(N)\ Q_{SS}(N)\ \Delta S(N) + q_S{}^T(N)\ \Delta S(N)\ \}\ ,$$

where $\mathbf{Q}_{ss}(k)$, $\mathbf{q}_s(k)$, $\mathbf{R}_{uu}(k)$, $\mathbf{r}_u(k)$, $\mathbf{Q}_{us}(k)$ are coefficient matrices defining a quadratic approximation of the original performance index. These matrices include the first and second partial derivatives of the $g_k[\ ]$ and $g_N[\ ]$ functions with respect to the state and control variables evaluated at the nominal sequences.

The perturbation control problem defined above is next solved to generate an optimal control sequence $\{\Delta\mathbf{u}^*(k), k=0,1, ..., N-1\}$. This constitutes the optimization direction which defines the new nominal control sequence according to the following relationship:

$$u^{new}(k) = u^0(k) + \alpha\ \Delta u^*(k)\ ,$$

$$k = 0, 1, \ldots, N-1\ ,$$

where α is the optimization step size. Some important features of the ELQG solution process are summarized below:

$ The ELQG iterations are (**1**) analytically-based (the optimization directions are obtained by Riccati-like equations), (**2**) reliable (the iteration process is guaranteed to converge if the problem has a feasible solution), and (**3**) computationally efficient (convergence is fast). In fact, in the neighborhood of the optimum, it can be theoretically shown that the method converges at a quadratic rate.

$ Control constraints are not included in the performance index as penalty terms but are handled *explicitly* through a Projected-Newton procedure. This has important computational efficiency implications as it allows for many constraints to enter or exit the binding control set at the same iteration. The optimization direction is then obtained in the space of the binding constraints.

One last complication is that in order to compute the control gains {D(k), L(k), Λ(k), k=0,1,...,N} one must already have the storage probability distribution. This, however, is resolved by adopting an iterative approach. Namely, the algorithm is first initiated with the Gaussian approximation approach described above, and a set of control gains is computed. Then, the storage traces are generated, and the process is repeated. Based on our experience, in two to three iterations, the probability distributions converge to their true forms and the procedure can terminate.

$ State (or, equivalently, elevation) constraints are handled through the barrier penalty functions discussed in the previous section. This approach has proven to be reliable and computationally efficient. Handling of the state constraints requires the characterization of the state probability density. A two-phase process is used for the state density computation. In the first phase, this density is approximated by its mean and covariance vector, respectively obtained by:

$$P_S(k+1) = F(k)\ \ P_S(k)\ F^T(k) + C(k)\, P_\xi(k)\ C^T(k)\ \ ,$$

$$F(k) = A(k) - B(k)\ \ D(k)\ \ L(k)\ \ ,$$

$$k = 0, 1, \ldots, N-1\ \ ,$$

where $\mathbf{P}_S(k)$ and $\mathbf{P}_\xi(k)$ are the state and input covariance matrices and {**D**(k), **L**(k), k=0,1,...,N-1} are control gains generated by the ELQG solution process. These gains represent a linear approximation of the true feedback laws and are used in the covariance computation to indicate that future decisions will take into consideration measurements of reservoir storage (feedback). The state mean and covariance are then used to construct a normal approximation of the state probability density and convert constraints into deterministic equivalents on the elevation mean:

$$Prob[\ H_i^{\min}(k) \le H_i(S_i(k))\ ] = \pi_i^{\min}(k)\ ,$$

$$Prob[\ H_i(S_i(k)) \le H_i^{\max}(k)\ ] = \pi_i^{\max}(k)\ ,$$

$$i = 1, 2, ..., n,\ \ k = 0, 1, ..., N\ .$$

$$\Phi_i^{\min}(k) \le \overline{H}_i(S_i(k)) \le \Phi_i^{\max}(k)\ ,$$

$$i = 1, 2, ..., n,\ \ k = 0, 1, ..., N\ ,$$

where $\{\Phi_i^{\min}\ ,\ \Phi_i^{\max}\}$ are the mean reservoir elevations such that

After the convergence of the first step, the generated control law is then applied to each inflow trace to generate the corresponding storage trace. With the generated storage traces, the probabilistic characteristics of the state variable are fully defined. The constraints and are updated. The second phase starts using the recalculated constraints until convergence.

The ELQG iterations continue until the value of the performance index can not be reduced any further. At this point the process terminates, and the current nominal control sequence becomes the problem solution. Under convexity conditions (which are valid in this formulation), this solution is globally optimal. (Convexity can be tested by starting the optimization process from different initial control sequences and verifying that the process converges at the same optimal sequence.)

As mentioned earlier, the control model is applied sequentially, where only the first element of the control sequence is actually applied. The system is then monitored, the new values of the state variables are recorded, and the optimization cycle is repeated at the beginning of the next (decadal) time period. In this way, the model always uses the most updated information regarding the system and continually Atunes@ its optimal policies to the current needs and conditions.

More details on the ELQG features can be found in the above-cited references.